Highlights

- Ordering of the intermetallic Fe40at%Al structure upon heating at different temperatures
- Use of the synchrotron radiation for the time-resolved evaluation
- Rietveld analysis for the evolution of fitting parameters to check strain tendency and growth of ordered domains.

Ordering Kinetics evaluation of FeAl powders

N. Cinca[1*], A. Isalgué[2], C. Auguet[2], A. Concustell[1], I.G. Cano[1], J. M. Guilemany[1], F. Fauth[3]

[1]Centre de Projecció Tèrmica, Fac. Química, Universitat de Barcelona, Diagonal 649 E-08028, Barcelona; Spain

[2] Dep. Física Aplicada, Universitat Politècnica Catalunya, Pla Palau 18 E-08003, Barcelona; Spain

[3]CELLS - ALBA Synchrotron. 08290 Cerdanyola del Valles, Barcelona

Contact details: ncincacpt2@gmail.com

Abstract

In this study, time resolved X-ray diffraction experiments using synchrotron X-ray radiation have been performed to get insight on the time and temperature dependent atomic ordering of an intermetallic Fe-40Al (at.%) ball-milled powder. The target of the present study is to gain knowledge on the rapid heating processes occurring during Thermal Spray coating processes. Present results show that in the temperature range 400ºC - 550ºC, the evolution of the order can be followed and modelled by fitting the powder diffraction patterns collected within the first minutes after fast heating. Reasonable refinements have been obtained by assuming the presence of two domains corresponding to the ordered and disordered lattices. The lattice constant changes from 0.29165±3 10^{-5} nm in the ball-milled powder at room temperature to 0.29281± 10^{-4} nm in the ordered phase after 3000s at 550ºC. The growth of the ordered phase is proposed to be a vacancy-related process with an activation energy of 1.04 eV. Above 550ºC, the ordering kinetics appears too fast to be resolved using the few seconds time scale of the present experiments which is in agreement to thermal spray results conditions.

Keywords: FeAl; synchrotron; ordering; x-ray; thermal spray; coating

1. Introduction

Ordering phenomena is a key process for the proper understanding of the outstanding properties that intermetallic compounds can offer in terms of mechanical, electrical and magnetic properties. This has been investigated for decades in the attempt to elucidate how slight changes on crystal lattice order result in changes on these properties [1, 2, 3].

The order-disorder transitions take place at a so-called critical ordering temperature T_c, which exists for either first or second-order phase transitions. At temperatures above T_c, a short-range order (SRO) parameter is defined and the atoms are prone to order over short distances only; below T_c, a long-range order (LRO) parameter, defined by the tendency of atoms to be surrounded by unlike atoms, shows a dependency on increasing the temperature i.e. it either decreases continuously like CuZn or drops abruptly to zero slightly above T_c like Cu_3Au [3].

Certain alloys possess the ordering temperature close to the melting temperature (T_m). Such alloys keep therefore a permanently ordered structure unless a special treatment such as high deformation by ball milling or high dose particle irradiation is applied [1]. Representatives of this group are Ni_3Al, NiAl, FeAl, TiAl; by contrast, examples of reversibly ordering alloys, whose $T_c < T_m$, can be found within Cu–Pt and Cu–Au systems [4]. From the first category, transition metal aluminides have been mainly investigated due to their low densities and promising high temperature oxidation resistance properties.

But how then is their degree of order affected upon fast heating up to almost the melting point followed by rapid cooling? This concept is interesting to elucidate what happens to Thermal Spray coating processes. These are a group of technologies where sufficient kinetic and thermal energy are imparted to the raw material (in powder, wire or rod form) to create a confined high-energy particle stream, and propel the energetic particles toward the substrate using a high-pressure carrier gas. The molten or partially molten particles deform on impact with the substrate creating cohesive bonds with each other and adhesive bonds with the substrate [5, 6]; even just kinetic energy can be transferred to the particles in the more recent less conventional Cold Gas Spray process, inducing solid-state bonding only by suitable plastic deformation of the material [7].

Due to the thermal history of the powder upon spraying, which can involve particle temperatures near the melting point of the material (specially in conventional processes) and afterwards high cooling rates upon impact onto the substrate, partial ordering can be obtained in intermetallic coatings [8]. The main motivation of this study is then to evaluate how fast a disordered intermetallic powder becomes ordered due to rapid heating, in analogy to what happens to particles in the flame. We expect to gain insight of time-temperature dependent atomic ordering in the processes involved during the spraying, oriented to improve the final properties. Since usual x-ray data acquisition with proper resolution takes a long time, synchrotron radiation will be used.

Nanocrystalline Fe-40Al (at.%) structures are obtained by thermal spray from a ball milled feedstock powder as a way to enhance mechanical properties. We have produced Fe-40Al (at.%) coatings by the high velocity oxy-fuel (HVOF) technology, obtaining good corrosion and oxidation resistance [9, 10]. Transition metal aluminides have strong potential for replacing superalloys and stainless steels in moderate and high temperature structural applications. FeAl-based alloys possess an outstanding high-temperature corrosion resistance [11] and they have a lower density (5.56g/cm^3) compared to other iron-based materials such as cast iron and stainless steels (e.g. in heating elements, hot-gas filters, piping and tubing, exhaust manifolds, etc.). However, some aspects such as poor room temperature ductility and toughness and mediocre creep strength, as well as fabrication difficulties have hindered the introduction of intermetallics in many cases as industrial structural materials [12]. Because of all these reasons, aluminides appear particularly interesting as coatings on more conventional higher-strength materials which are less corrosion-resistant at high temperatures.

Many works have dealt with the order-disorder transitions in the Fe-Al system in terms of structural changes upon temperature, mainly through magnetic, calorimetric and X- ray diffraction experiments, showing complementary results with these techniques [13, 14]. Some authors have pointed out that the strength of ordering behavior of late transition-metal aluminides finds its origin in the atomic size effect, since the reduction in strain energy due to atomic size misfit can be achieved by ordering. However, the validity of this size effect has also been questioned for years [15].

Owing to long data acquisition, conventional laboratory X-ray sources present serious limitations for the study of how the order parameter in thermal equilibrium varies with temperature. On the other hand, the high intensity offered by synchrotron X-ray radiation sources coupled with modern fast timing detectors, allows getting insight on the kinetics of time-temperature atomic ordering processes. Such techniques are being applied for investigating the ordering transitions [16, 17, 18, 19] as well as the evaluation of several material crystallization kinetics [20, 21, 22, 23] and other reactions [24, 25, 26, 27]. In their work on Cu_3Au, Shannon et al., studied the order-disorder transition starting from a disordered state at an initial temperature T_i above the critical one ($T_i > T_c$) and then quenching into a region of the phase diagram where the equilibrium state is ordered ($T_c > T_f$), T_f standing for final temperature [19]. By contrast, Schaefer et al., performed some time dependent experiments for Fe-45Al (at.%) specimens by using time-differential length scale measurements after fast heating rates and then left isothermally treated; they obtained the vacancy formation and migration enthalpies, 1.0 ± 0.1 eV and 1.5 ± 0.2 eV respectively [28]. The purpose of the present study is to report the ordering process in a Fe-40Al (at.%) ball milled powder alloy upon fast heating from the room temperature disordered state and, to evaluate the kinetics of such ordering process as well. As mentioned above, this will help with the understanding of the ordered phase formation in thermal spraying.

2. Experimental method

A ball milled Fe-40Al (at.%) alloy powder supplied by CEA-DTEN (Grenoble) was used for this study. It has a nominal composition of Fe–40Al–0.05Zr (at.%) +50 ppm B+1 wt%.Y_2O_3.

The temperature dependent and time resolved powder diffraction experiments were performed on the BL04-MSPD beamline of the synchrotron facility ALBA located in the Barcelona area [29, 30].

The powders were enclosed into sealed quartz capillaries of 0.5 mm diameter, and the data was collected in transmission geometry using a monochromated beam of 0.042492 nm wavelength. The set-up included a remote controlled heated air blower (Cyberstar) allowing collecting data at the selected sample temperatures 400, 450, 500, 550, 600, 650, 700 and 750ºC after fast heating from room temperature. The hot spot of the blower, this is the constant temperature range of the sample, is 5 mm in length and the X-ray beam was 3 x 0.7 mm^2. The time needed for the blower to go from room temperature to the selected data acquisition temperature was about 3-5 min, also considering a non-negligible temperature overshoot of ~5%. The analogy to thermal spray

appears as an approximation to the process since the powder is heated when fed in the flame and high temperatures are reached in very short times. To avoid the higher temperatures due to the overshoot, the following methodology was applied. The sample was rapidly heated at the blower set temperature and left stabilized during ~ 10min. It was then remotely moved 10 mm (10s moving time) from that position to heat another portion of the sample. By operating in this way, the part of the sample studied was quickly heated at the selected temperature without suffering from temperature overshoot. It was checked that, at that zone 10 mm apart from the initial heated position, the atomic order did not change, even testing at the highest temperature. The time for the 0.5 mm diameter capillary to achieve the final temperature, when laterally moved and exposed to the hot air flow, was estimated to be around 10 s. Sufficiently good data statistics could be obtained with 5 s effective acquisition time, which taking into account data processing/transfer and temperature reading resulted in 8.2s time resolution of our X-ray powder data collection. The powder patterns were registered using the position sensitive MYTHEN detector (6 single modules of 1280 channels) allowing collecting in a single shot a 41.1º 2θ angular range in 0.0062º steps. Between two detector modules, the pattern is obscured over a ~0.2 º angular range; it was hence crucial for time resolved experiments to smartly position the detector so to avoid Bragg reflections on this specific "dead" regions. The X-ray diffractograms will be presented in reciprocal space units instead of the 2θ scattering angle:

Equation 1: $Q = 4\pi(\sin\theta)/\lambda$

The X-ray patterns were refined by the Rietveld method using the FullProf software [31]. For this work, we assumed the presence of different domains corresponding to a completely ordered bcc B2 superlattice and a completely bcc disordered phase [32, 33]. Since ordering parameters are related to the microstructure (strain and size), a particular attention was focused on the analysis and fitting of the x-ray peak shapes; for that purpose, we used the Thomson-Cox-Hastings pseudo-Voigt function [32]. The instrumental resolution was determined by collecting data of a $Na_2Ca_3Al_2F_{14}$ sample enclosed in 0.5mm diameter capillary.

In order to achieve a good correlation between the calculated and the experimental diffractograms, the minimum values of the usual fit indicators of the FullProf software were monitored. The increase of peak full width at half maximum (FWHM) respect to the instrumental contribution is assumed to come mainly from the grain size and strain effects; the different parameters were fitted throughout the refinement. At each step, iteration cycles were conducted until convergence was reached.

The full widths at half maximum H_G and H_L of the corresponding Gaussian (Eq 2) and Lorentzian (Eq 3) contributions are calculated according to an angular dependence [23]:

Equation 2: $$H_G^{\,2} = [U + (1-\xi)^2 D_{ST}^{\,2}(\alpha_D)]tg^2\theta + Vtg\theta + W + \frac{I_G}{\cos^2\theta}$$

Equation 3: $$H_L = [X + \xi D_{ST}(\alpha_D)]tg\theta + \frac{[Y + F(\alpha_Z)]}{\cos\theta}$$

Where U, α_D, X are terms related to strain and, Y, I_G, α_Z are related to domain size. According to the FullProf manual, the parameter ξ is a mixing coefficient to mimic Lorentzian contribution to strains. The output *.mic files give further information about microstructural parameters from each diffraction peak.

The approximate sizes of the ordered and disordered domains have been found according to the fitted Lsize (FullProf size parameter) as follows, due to the units used on the data:

Equation 4: Broadening contribution (1/nm)=(fitted *Lsize*)/2π

Equation 5: Size(nm)=100/(fitted *Lsize*)

3. Results and discussion

The atomized Fe-40Al (at.%) powder had a spherical morphology. Figure 1 presents a micrograph of the ball-milled Fe-40Al (at.%) powder, with characteristic irregular morphology corresponding to the milling process. Figure 2 shows the X-ray diffraction pattern of as-atomized powder and of atomized+ball-milled

powder, at room temperature. The pattern of the atomized powder at room temperature was obtained by collecting at several detector positions hence covering the gap mentioned in the previous section (Fig. 2).

The atomized powder (Fig. 2a) showed the presence of all peaks corresponding to the ordered bcc B2 structure. The fitted B2 cell parameter at room temperature was 0.28972±2 10^{-5} nm. However, for the ball-milled powder at room temperature, no peaks corresponding to ordering (indexed as hkl, with h+k+l=odd) were observed. Figure 2b corresponds to the ball-milled x-ray diffraction at room temperature, just showing the corresponding fundamental lines (h+k+l=even). The peaks are observed to be broad, indicating that milling induces strain and grain refinement.

The corresponding lattice constant of the ball-milled powder at room temperature was found to be 0.29165±3 10^{-5} nm by the refinement. Zamanzade et al., have recently published in their review, the comparison between the lattice parameter for the α-Fe (bcc, $a_0 = b_0 = c_0 = 0.28665$ nm) with the values found by many authors in the literature for the B2-FeAl phase ($a_0 = b_0 = c_0 = 0.291, 0.283, 0.3031$ nm) [34]. The slightly larger lattice parameter compared to that of the B2 phase points out the lower degree of order as a result of the heavy plastic deformation.

Most works about B2-ball-milled intermetallic phases have also yielded a disordered ~~A2~~ solid solution structure [35, 36, 37]. In addition, non-stoichiometric compositions of FeAl (greater or less than 50 at.% Al) lead to the generation of constitutional defects. The sub-lattices of the B2 structure are defined as the α sublattice containing Fe atoms and the β sublattice containing Al atoms. Four possible defects can be created on these sublattices: (i) Fe atoms on the β sublattice (anti-site Fe atoms), (ii) Al atoms on the α sublattice (anti-site Al atoms) and (iii) vacancies on the α or β sublattice. FeAl is actually considered a less strongly ordered intermetallic because of the more complex defect distribution, where in addition to the occurrence of vacancies at the Fe site, the substitutional antisite defects at the Fe sites can also be very stable [38]. Both effects, the off-stoichiometric composition with 40at%Al and the ball milling process, generate a distorsion within the lattice resulting in such increased lattice parameter. Actually, it has been shown that the NiAl phase continues to be in the ordered state upon milling without getting disordered, whereas the FeAl phase was found to be in the disordered state both in the as-produced condition by ~~MA~~ mechanical alloying and also on milling the ordered compound [39, 40]. With short time at the temperature of 400ºC and above, the fundamental peaks first appear very broad due to the strain effects of the ball milling, but they become narrower as the disordered phase disappears and the ordered phase appears (Fig 3).

At first attempt, the occupation of Fe and Al were made variable, maintaining the chemical composition of the phase. No satisfactory fitting was achieved; the width of peaks is large, and no good fitting concerning the shape of peaks was obtained. A different peak width evolution for the superlattice and fundamental peaks was observed; due to all this, a variable width fitting procedure for superstructure peaks (hkl, h+k+l=odd) was attempted; this improves the fitting but the shape of peaks was not in good agreement (RBragg larger than 10). Relatively wide peaks without specific correlation among their widths at intermediate times at the selected annealing temperatures suggested the presence of two phases. Thus, we assumed the presence of different domains, corresponding to a completely ordered B2-type phase and a completely disordered; then, the refinement was approached by defining these two phases with the introduction of the proper (fixed) occupancy factors from the start. Therefore, the main parameters under considerations and indicative of the (dis-) ordering kinetics finally were: (i) the ratio between the ordered and disordered phase, being defined as the ratio between the two refined scale factors, (ii) the evolution of both cell parameters at the tested temperatures, (iii) the strain contribution of the remaining disordered phase and (iv) the domain size evolution of the two phases. The starting ball-milled powder showed only disordered phase, while on short times (a few seconds) of annealing time, the ordered phase increased its percentage.

Figure 4 shows the evolution of the ordered (a) and disordered (b) cubic phases cell parameters at the different temperatures along the experiment, when it is assumed that both phases have already stabilized. Very slight changes can be observed. Table 1 indicates the minimum value of the usual fit indicators (Chi^2, RBragg) that were monitored by the FullProf software along the fitting [32].

Table 1. Values of the fit indicators

Temperature (ºC)	RBragg disordered phase	RBragg ordered phase	Chi^2 range
400	1.1	2.5	11-15
450	1.2	1.5	8-12
500	2	1.9	5-9
550	1.4	1.6	6-10

The ordered phase stabilizes after 3000s at around 0.29184 ±3 10^{-5} nm, 0.29216± 4 10^{-5} nm, 0.29244± 3 10^{-5} nm, and 0.29281± 10^{-4} nm at the temperatures of 400, 450, 500 and 550ºC respectively, whereas the disordered phase presents more scattered values due to its reduced occurrence at long times of annealing treatment. A coefficient of thermal expansion of 2.2 10^{-5} K^{-1} is obtained, coherent with the one obtained from the cell parameter fits for the atomized powder at room temperature and at 500ºC (2.1 10^{-5} K^{-1}).

Figure 5 shows the mass% of the ordered phase calculated from the ratio between the refined scale factors of the measurements. It can be observed that at 400ºC, the ordering process takes place more slowly, as expected, than at 450ºC and above; actually, it does not seem that even after the test time the complete ordering is achieved. Thermal energy promotes diffusion, which induces Fe and Al atoms to occupy their most energetically favorable positions, but at temperatures below 500ºC, the thermal energy input is still low to promote almost full ordering and, at even much higher temperatures, the thermal vibration is becoming a competitive process, thus also limiting the formation of the complete ordered structure [13]. At 500 and 550ºC, the ordering occurs fast and the material appears completely ordered after some 200 s. At above such temperature, the ordering occurs during the first 10-30s and, considering that the acquisition is done every 8 s, no much change can be observed after two diffractograms. The time dependence of the ordered phase weight% can be fitted to an exponential behavior approaching 100% at long times, and the following time constants were obtained: 400ºC, 910 s; 450ºC, 450s; 500ºC, 58 s; and 550ºC, 47 s. By plotting the natural logarithm of the time constants as function of the inverse absolute temperature, the obtained activation energy for the process was equivalent to 1.04 eV. Then, as this value is very near the energy determined by Schaefer et al. (1.07 eV) for the formation of vacancies, it appears that the growth of the ordered phase could be a vacancy-related process [29].

In Figure 6, the ordering process results in a release of strain can be seen. Also table 2 shows the range of values corresponding to the strain parameter (X, see equation 3) as well as the strain. The disordered arrangement produced by ball milling is a metastable, highly strained state. Thermal energy promotes diffusion, which induces Fe and Al atoms to occupy their most energetically favorable positions, eventually leading to an ordered phase; however, some strain remains, which should be related to a more long-range (and more time involved) process (large defects involved). The strain releases slowly after the ordering process because of the long range diffusion needed.

Table 2. Strain and Size fitted parameters

Temperature (ºC)	X	Strain (%)	Fitted LSize2
400	0.7-0.85 +/-0.003	0.48-0.58	3-15 +/- 0.3
450	0.65-0.9 +/-0.003	0.44-0.62	3-12 +/- 0.5
500	0.5-0.8 +/-0.003	0.34-0.55	2.5-9 +/- 0.4
550	0.48-0.65 +/-0.002	0.33-0.45	2.4-3.5 +/- 0.2

By considering the ordering through the existence of individual ordered domains that develop either when temperature or time are increased, they grow more rapidly at 500ºC and 550ºC. Reordering after a severe plastic deformation process has been actually reported to occur upon heating by the coarsening of the nanodomains until the ordered domains reach the size of the grains [41].

There are two modes of defect structures in the B2 crystal: anti-structure defect structure and triple defect structure. The anti-structure defect structure results in an anti-site atom for a constitutional defect of a rich phase, and a pair of anti-structure defects for thermal defects. The triple defect structure consists of anti-site Fe atoms for Fe-rich constitutional defects and sublattice vacancies for Al-rich constitutional defects. The situation is actually complicated for the less strongly ordered FeAl. In addition to the occurrence of vacancies at the Fe site, the substitutional antisite defects at the Fe sites can also be very stable. Given the ΔH_f value for FeAl, it is

situated on the borderline for the different defect structures. However, Pike [42] shows that the triple vacancy model predicts the vacancy concentration of FeAl. The results here are coherent with Pike's.

A fast growing of ordered phase domains is observed from the fittings. From no detectable existence, to some 8 nm size in 8 s at 450ºC (see figure 7 and 8 as well as table 2). This part would correspond to shorter range of order. At longer times, once the order is near completed, the size continues to grow, but more slowly, as it would correspond to long range diffusion.

Concerning thermal spray processes, we should consider how this degree of order attained at the temperature reached by the particle feedstock material (partially or fully molten droplet), is then maintained upon the high cooling rates up to 10^6 K/s that are involved. First, the temperatures studied in the present work would be similar to the temperatures reached at the core of coarse particles, leading to their recrystallization and partial ordering, while the particle shells reach up to the melting point of the material. Cordier-Robert et al. actually confirmed that the non-homogeneous atomic order state in High Velocity Oxygen Fuel and Atmospheric Plasma Spray coatings depends on the initial powder microstructure in the feedstock [43]. Core is more ordered than shell in the case of the atomized ~~Fe60Al40~~ Fe-40Al (at.%) powder and vice versa for the milled ~~Fe60Al40~~ Fe-40Al (at.%) powder. All these results would be in agreement to what was previously stated that these intermetallics do not usually disorder upon rapid quenching in the core. The molten areas are another issue, which cannot be explained by the experiments presented here and, where the behavior of the undercooled material must be considered.

4. Conclusions

The study of the time-temperature atomic ordering for a Fe-40Al (at.%) ball milled alloy by means of X-ray synchrotron powder diffraction results in the following conclusions:

- The 400-550ºC temperature range can be followed by the experimental setup (the time to reach the temperature of the sample is about 10 s); one diffractogram was acquired each 8.2 s.
- The best fitting is performed by considering the presence of different domains (ordered and disordered phase, fixed occupancy factors), one growing and the other diminishing. The results seem to indicate that this assumption is the best one.
- At 400ºC, the ordering process takes place more slowly (some hours), as expected, than 450ºC and above (some minutes, or some seconds above 500ºC).
- The increase of ordered phase amount can be fitted to an exponential behavior. At long times, the ordering appears to be completed at 450ºC and above, although the existence of some strain even at high temperatures may indicate that some is not completely released. This shows a short-range process, seemingly related to vacancies (because the 1.04 eV value found for the activation energy is near to the reported in the literature for the formation of vacancies) for the ordering; at larger atomic distances, additional time process for the relief of residual strains (seemingly related to larger defects) may explain the results.
- The fitted growth of ordered phase domain size seems to follow the above indicated process.
- Even the small in-flight time of the particles in a HVOF process is enough to produce certain order of the internal core structure, which does not disorder upon rapid cooling. The ordering process is however assumed to be too fast to be able to be resolved in the time scale of the present experiments (a few seconds).

Acknowledgements

The authors acknowledge the ALBA synchrotron project 2012100439, "FeAl powders for thermal spray coatings: Ordering Kinetics evaluation", carried out at beam line BL04 – MSPD.

The research leading to these results has received funding from the People Programme (Accions Marie Curie) of the 7 Framework Programme of the European Union (FP7/2007-2013) under REA grant agreement no. 600388 (TECNIOspring programme), and from the Agency for Business Competitiveness of the Government of Catalonia, ACCIÓ.

Figure captions

Figure 1. SEM picture showing the morphology of ball milled Fe-40Al (at.%).
Figure 2. Synchroton X-ray diffraction patterns of the two Fe-40Al (at.%) powders tested at room temperature: (a) atomized powder and (b) ball-milled powder. The corresponding Q values are 18.054 nm^{-1} at $2\theta=7^{o}$ and 93.838 nm^{-1} at $2\theta=37^{o}$.
Figure 3. Time evolution of diffraction spectra for ball milled Fe-40Al (at.%) at 400ºC: at room temperature (RT), after 8.2 s, after 172 s and, after 1558 s at 400ºC.
Figure 4. Cell parameter evolution versus time at the different temperatures for the (a) ordered phase and (b) disordered phase respectively.
Figure 5. Time evolution of the ordered phase weight percentage (a) at 400ºC; (b) at 450ºC; (c) at 500ºC; (d) at 550ºC.
Figure 6. Strain and strain parameter X as a function of time: (a) at 400ºC; (b) at 450ºC; (c) at 500ºC; (d) at 550ºC.
Figure 7. Fitted size parameters as a function of time: (a) 400ºC, (b) 450ºC, (c) 500ºC and (d) 550ºC. Fitted *Lsize1* refers to the size parameter for disordered domains, fitted *Lsize2* refers to the size parameter for the ordered domains.
Figure 8. Dimensions of ordered phase domains from the size parameters in fig 7.

References

[1] Pfeiler W., Ordering Phenomena in Alloys: Access to Kinetic Parameters and Atom-Jump Processes, JOM-J. Met. 2000;52(7):14-8.

[2] Cahn R. W., Intermetallics: new physics, Contemporary Physics, 2001;42(6):365-75.

[3] Porter D., Phase transformations in metals and alloys, 2nd ed., Van Nostrand Reinhold, New York, 1981.

[4] Pfeiler W., Sprusil B., Atomic ordering in alloys: stable states and kinetics, Mater. Sci. Eng. A 2002; 324:34–42.

[5] Davis J.R., Handbook of Thermal Spray Technology, ASM International, OH, 2004.

[6] Pawlowski L., The science and engineering of Thermal Spray coatings, John Wiley & Sons, New York, 1995.

[7] Maev R. Gr., Leshchynsky V., Cold Gas Dynamic Spray, CRC Press, ISBN 9781466584426

[8] Cinca N., Dosta S., Guilemany J.M., Nanoscale characterization of FeAl-HVOF coatings, Surf. Coat. Technol. 2010;205:967–73

[9] Guilemany J.M., Lima C.R.C., Cinca N., Miguel J.R., Studies of Fe–40Al coatings obtained by high velocity oxy-fuel, Surf. Coat. Technol. 2006; 201:2072-79.

[10] Guilemany J. M., Cinca N., Dosta S., Lima C., High-temperature oxidation of Fe40Al coatings obtained by HVOF thermal spray, Intermetallics, 2007;15:1384-94.

[11] Liu C. T., Stiegler J. O.. Ordered intermetallics. In: Properties and selection: nonferrous alloys and special purpose materials. Metals Handbook. Properties and selection: nonferreous alloys and special-purpose materials. 10th ed., vol. 2. ASM International; 1990.

[12] Morris D. G., Muñoz-Morris M. A., Intermetallics: past, present and future, Revista de Metalurgia 2005:498-501

[13] Guilemany J. M., Cinca N., Casas Ll., Molins E., Ordering and disordering processes in MA and MM intermetallic iron aluminide powders, J. Mater. Sci. 2009;44: 2152-61.

[14] Gialanella S., Amils X.,,M. Baró D., Delcroix P., Le Caër G., Lutterotti L., Surinaach S., Microstructural and kinetic aspects of the transformations induced in a FeAl by ball milling and thermal treatments, Acta Mater. 1998;46(9):3305-16.

[15] Fu C. L., Origin of ordering in B2-type transition-metal aluminides: Comparative study of the defect properties of PdA1, NiA1, and FeA1, Phys. Rev. B 1995;52(5):3151-8

[16] Yeoh, L.A., Liss, K.-D., Bartels, A., Chladil, H., Avdeev, M., Clemens, H., Gerling, R., Buslaps, T., In situ high-energy X-ray diffraction study and quantitative phase analysis in the alpha plus gamma phase field of titanium aluminides. Scr. Mater. 2007;57:1145–48.

[17] Watson, I.J., Liss, K.-D., Clemens, H., Wallgram, W., Schmoelzer, T., Hansen, T.C., Reid, M., In Situ Characterization of a Nb and Mo Containing gamma-TiAl Based Alloy Using Neutron Diffraction and High-Temperature Microscopy. Adv. Eng. Mater. 2009;11: 932–7

[18] Liss, K.-D., Whitfield, R.E., Xu, W., Buslaps, T., Yeoh, L.A., Wu, X., Zhang, D., Xia, K., In situ synchrotron high-energy X-ray diffraction analysis on phase transformations in Ti-Al alloys processed by equal-channel angular pressing. J. Synchrotron Radiat. 2009;16: 825–34.

[19] Shannon R. F., Nagler S. E., Harkless C. R., Time-resolved x-ray-scattering study of ordering kinetics in bulk single-crystal Cu3Au, Phys. Rev. B 1992;46(1):40-54.

[20] Dos Santos D.S, Crystallization kinetics of Fe–B–Si metallic glasses, J. Non-Cryst. Solids 2002;304:56–63.

[21] Natter H., Schmelzer M., Loffler M.-S, Krill C. E., Fitch A., Hempelmann R., Grain-Growth Kinetics of Nanocrystalline Iron Studied In Situ by Synchrotron Real-Time X-ray Diffraction, J. Phys. Chem. B 2000;104:2467-76.

[22] Torrens-Serra J., Peral I., Rodriguez-Viejo J., Clavaguera-Mora M.T., Microstructure evolution and grain size distribution in nanocrystalline FeNbBCu from synchrotron XRD and TEM analysis, J. Non-Cryst. Solids 2012;358:107–13.

[23] Wang X.-L., Almer J., Liu C. T., Wang Y. D., Zhao J. K., Stoica A. D., Haeffner D. R., Wang W. H., In situ Synchrotron Study of Phase Transformation Behaviors in Bulk Metallic Glass by Simultaneous Diffraction and Small Angle Scattering, Phys. Rev. Letters 2003;91(23):4 pp.

[24] Yan, K., Carr, D.G., Kabra, S., Reid, M., Studer, A., Harrison, R.P., Dippenaar, R., Liss, K.-D., In Situ Characterization of Lattice Structure Evolution during Phase Transformation of Zr-2.5Nb. Adv. Eng. Mater. 2011;13:882–6.

[25] Rakha, K., Beladi, H., Timokhina, I., Xiong, X., Kabra, S., Liss, K.-D., Hodgson, P., On low temperature bainite transformation characteristics using in-situ neutron diffraction and atom probe tomography. Mater. Sci. Eng. A 2014;589: 303–309.

[26] Sedmák P., Šittner P., Pilch J., Curfs C. , Instability of cyclic superelastic deformation of NiTi investigated by synchrotron X-ray diffraction, Acta Materialia 2015;94:1:257–70

[27] Chen, G., Liss, K.-D., Cao, P., An in situ Study of NiTi Powder Sintering Using Neutron Diffraction. Metals 2015;5:530–46.

[28] Schaefer H.-E., Frenner K., Würschum R., Time-Differential Length Change Measurements for Thermal Defect Investigations: Intermetallic B2-FeAl and B2-NiAl Compounds, a Case Study, Phys. Rev. Letters 1999;82(5):948-51.

[29] Fauth F., Peral I., Popescu C., Knapp M., The new material science powder diffraction beamline at ALBA synchrotron, Powder Diffr. 2013; 28:S360-70

[30] Fauth F., Boer R., Gil-Ortiz F., Popescu C., Vallcorba O., Peral I., Fullà D., Benach J., Juanhuix J., The crystallography stations at the Alba synchrotron, Eur. Phys. J. Plus 2015;130:160:1-13

[31] FullProf2000. Juan Rodríguez-Carvajal, Laboratoire Léon Brillouin (CEA-CNRS), CEA/Saclay, 91191 Gif sur Yvette Cedex, FRANCE. [31] https://www.psi.ch/sinq/dmc/ManualsEN/fullprof.pdf

[32] Allen S. M., Cahn J. W., A microscopic theory for antiphase boundary motion and its application to antiphase domain coarsening, Acta Metal. 1979;27(6):1085-95

[33] Cahn J. W., Allen S. M., A microscopy theory for domain wall motion and its experimental verification in Fe-Al alloy domain growth kinetics, J. Phys. Colloques 1977;38C7:51-4

[34] Zamanzade M., Barnoush A., Motz C., A Review on the Properties of Iron Aluminide Intermetallics, Crystals 2016;6:29 pp.

[35] Amils X., J. Garitaonandia S., Nogués J., Suriñac S., Plazaola F., Muñoz J. S., Baró M. D., Micro and macroscopic magnetic study of the disordering (ball milling) and posterior (annealing) of Fe-40at%Al, J Non-Cryst Solids 2001;287:272-6

[36] Apiñaniz E., Garitaonandia J. S., Plazaola F., Influence of disorder on the magnetic properties of FeAl alloys: theory, J Non-Cryst Solids 2001;287:302-7.

[37] Meyer M., Mendoza-Zelis L., Sánchez F. H., Mechanical milling of the intermetallic coimpound AlFe, Phys. Rev. B 1999;60(5):3206-12

[38] Fu C. L., Origin of ordering in B2 type transition metal aluminides: comparative study of the defect properties of PdAl, NiAl and FeAl, Phys. Rev. B 1999;22(5):3151-58.

[39] Schropf H, Kuhrt C, Arzt E, Schultz L. Scripta Metall. Mater. 1994;30:1569-74.

[40] Suryanarayana C., Mechanical alloying and milling, Prog Mater Sci 2001;46:1-184

[41] Gammer C., Mangler C., Karnthaler H.P., Rentenberger C., Growth of nanosized chemically ordered domains in intermetallic FeAl made nanocrystalline by severe plastic deformation, Scripta Mater. 2011;65: 57–60

[42] Pike LM. The effects of ternary alloying on the defect structure and mechanical properties of B2 compounds. PhD thesis, University of Wisconsin-Madison, 1998.

[43] Cordier-Robert C., Grosdidier T., Gang J., Foct J., Mössbauer and X-ray diffraction characterization of Fe60Al40 coatings prepared by thermal spraying, Hyperfine Interact 2006;168:951–7

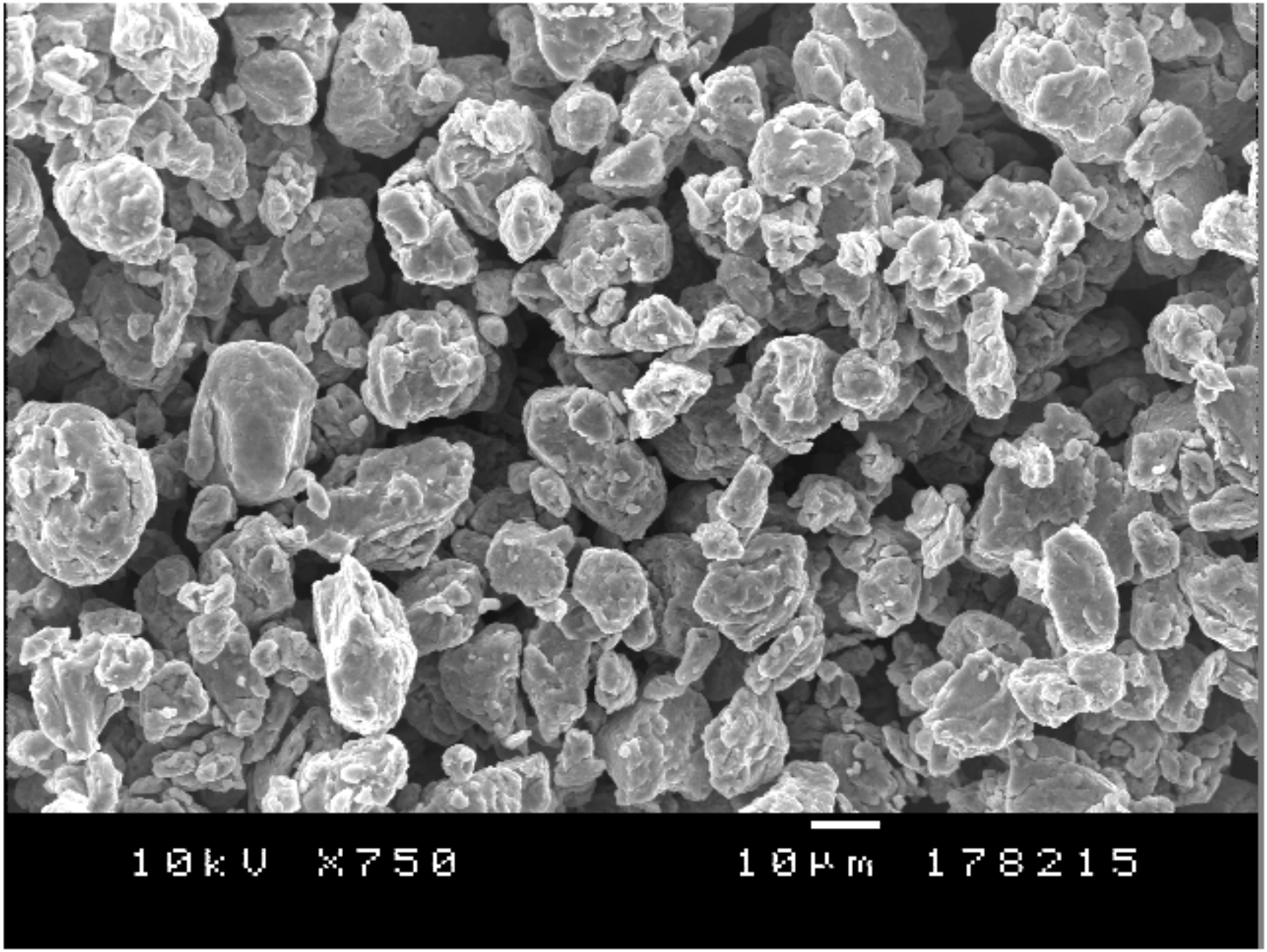
10kV X750
10µm 178215

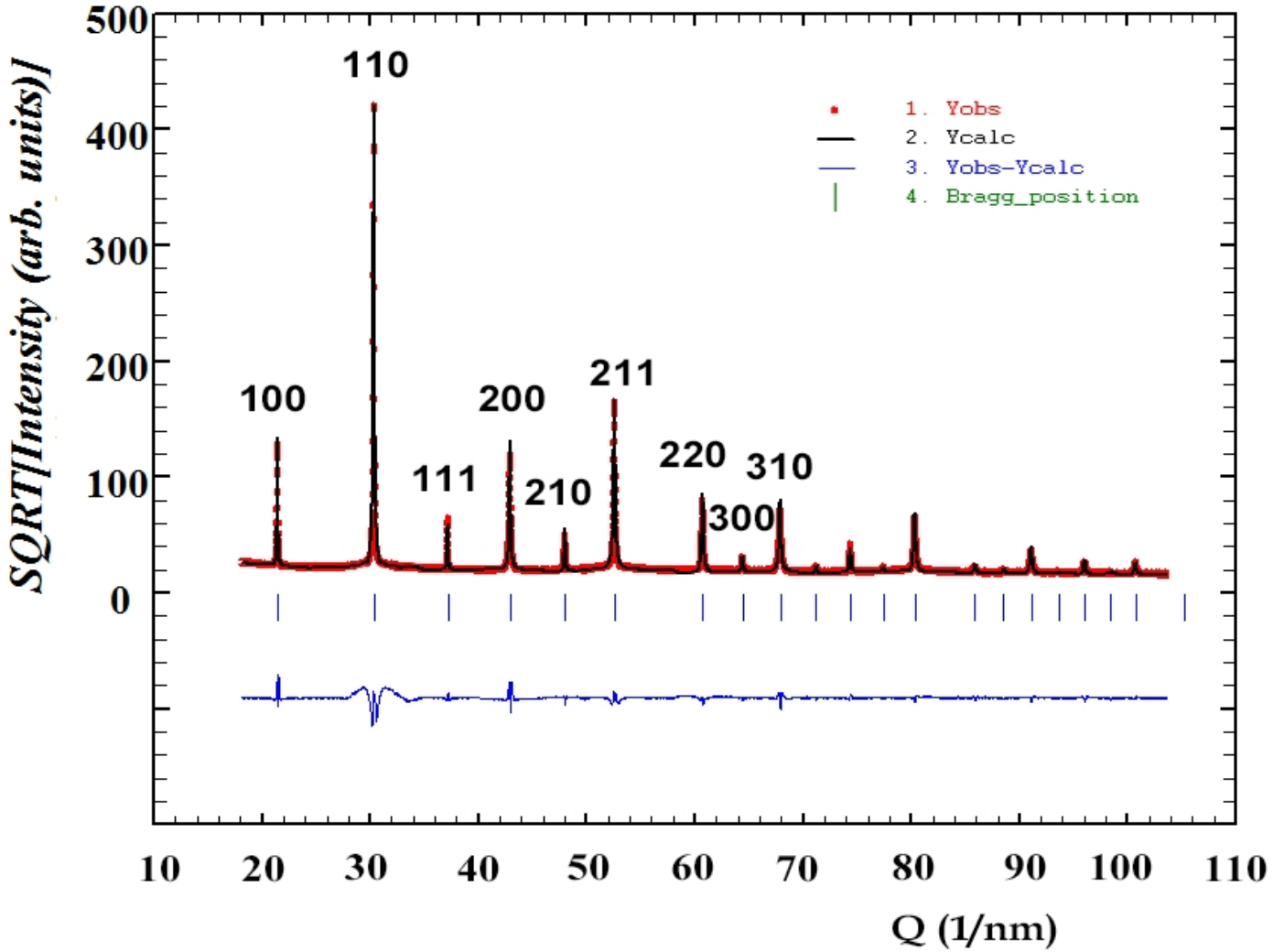
SQRT[Intensity (arb. units)]
500
400
300
200
100
0
10
20
30
40
50
60
70
80
90
100
110
Q (1/nm)
1. Yobs
2. Ycalc
3. Yobs-Ycalc
4. Bragg_position
100
110
111
200
210
211
220
300
310

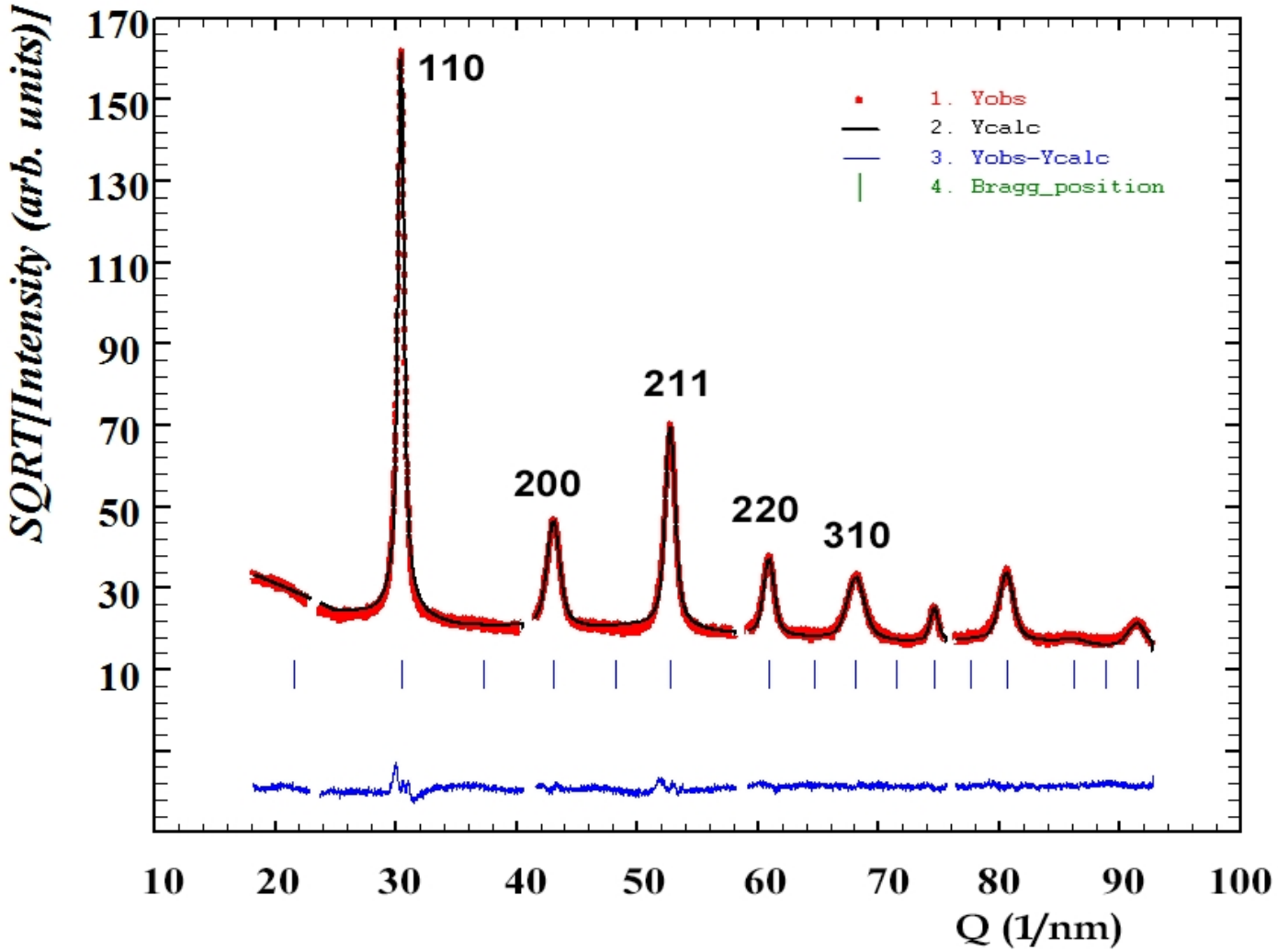
SQRT[Intensity (arb. units)]
170
150
130
110
90
70
50
30
10
110
200
211
220
310
1. Yobs
2. Ycalc
3. Yobs-Ycalc
4. Bragg_position
10
20
30
40
50
60
70
80
90
100
Q (1/nm)

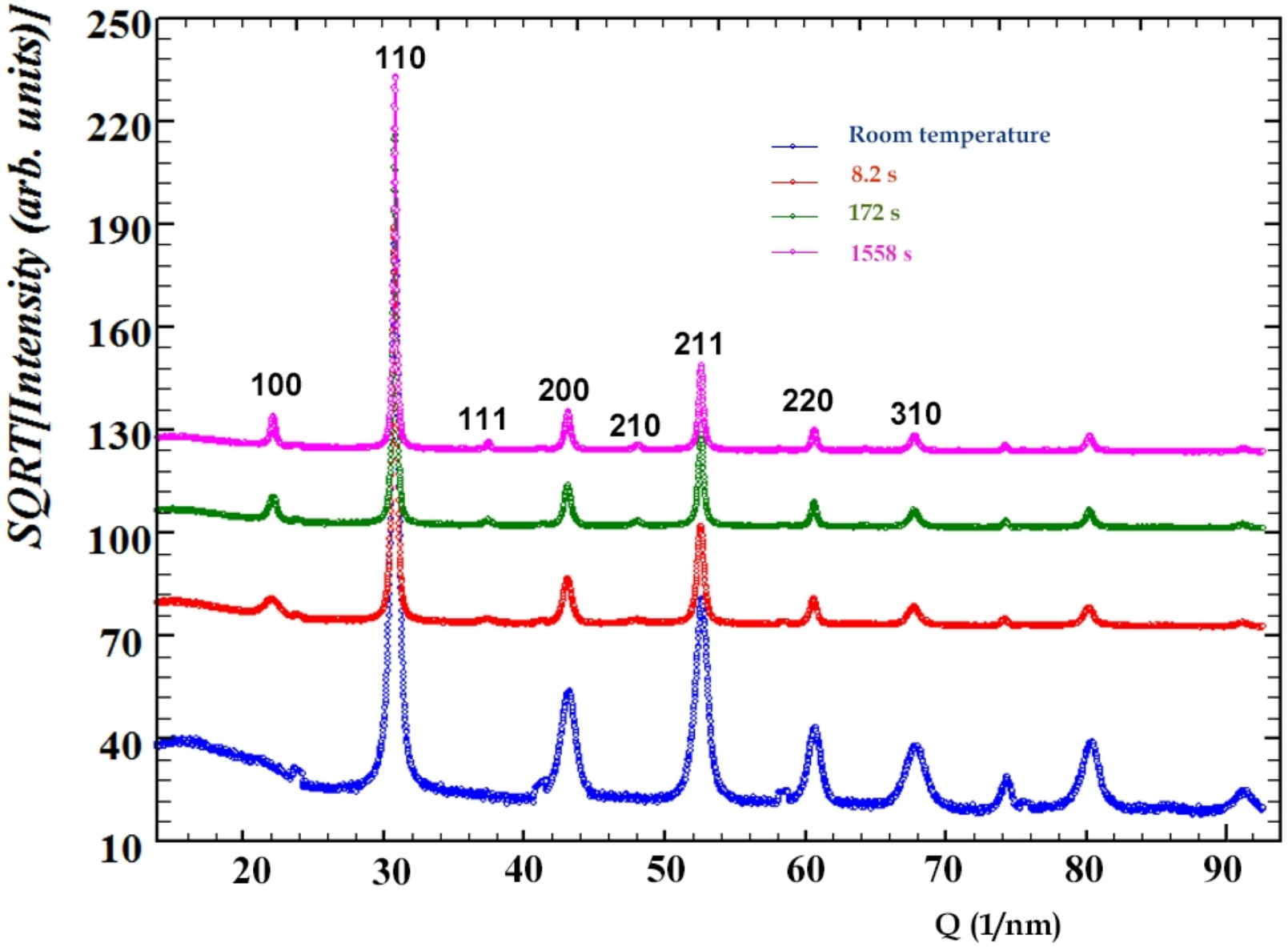
SQRT[Intensity (arb. units)]
250
220
190
160
130
100
70
40
10
20
30
40
50
60
70
80
90
Q (1/nm)
110
100
111
200
210
211
220
310
Room temperature
8.2 s
172 s
1558 s

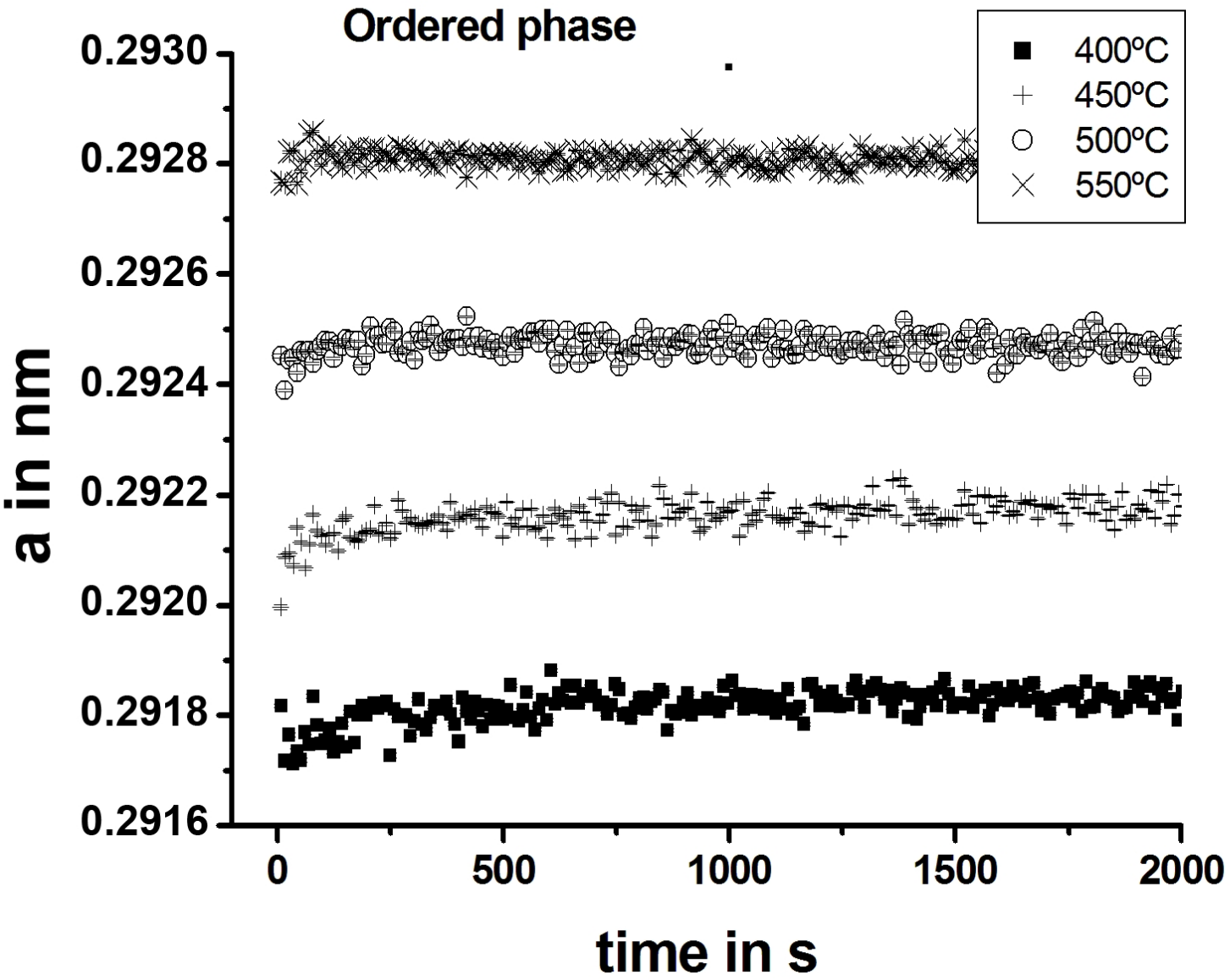
Ordered phase
400ºC
450ºC
500ºC
550ºC
0.2930
0.2928
0.2926
0.2924
0.2922
0.2920
0.2918
0.2916
a in nm
0
500
1000
1500
2000
time in s

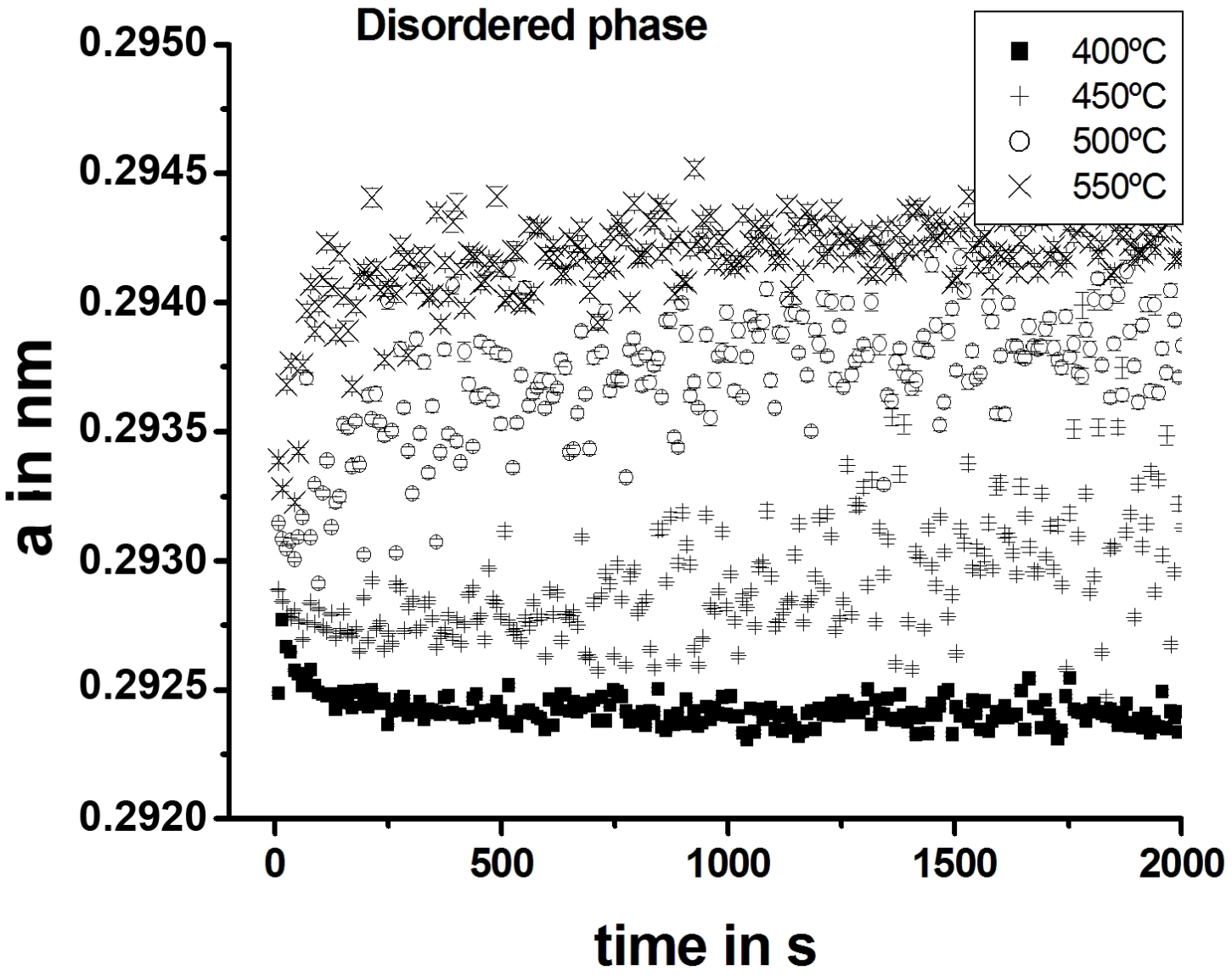
Disordered phase
400ºC
450ºC
500ºC
550ºC
a in nm
0.2950
0.2945
0.2940
0.2935
0.2930
0.2925
0.2920
0
500
1000
1500
2000
time in s

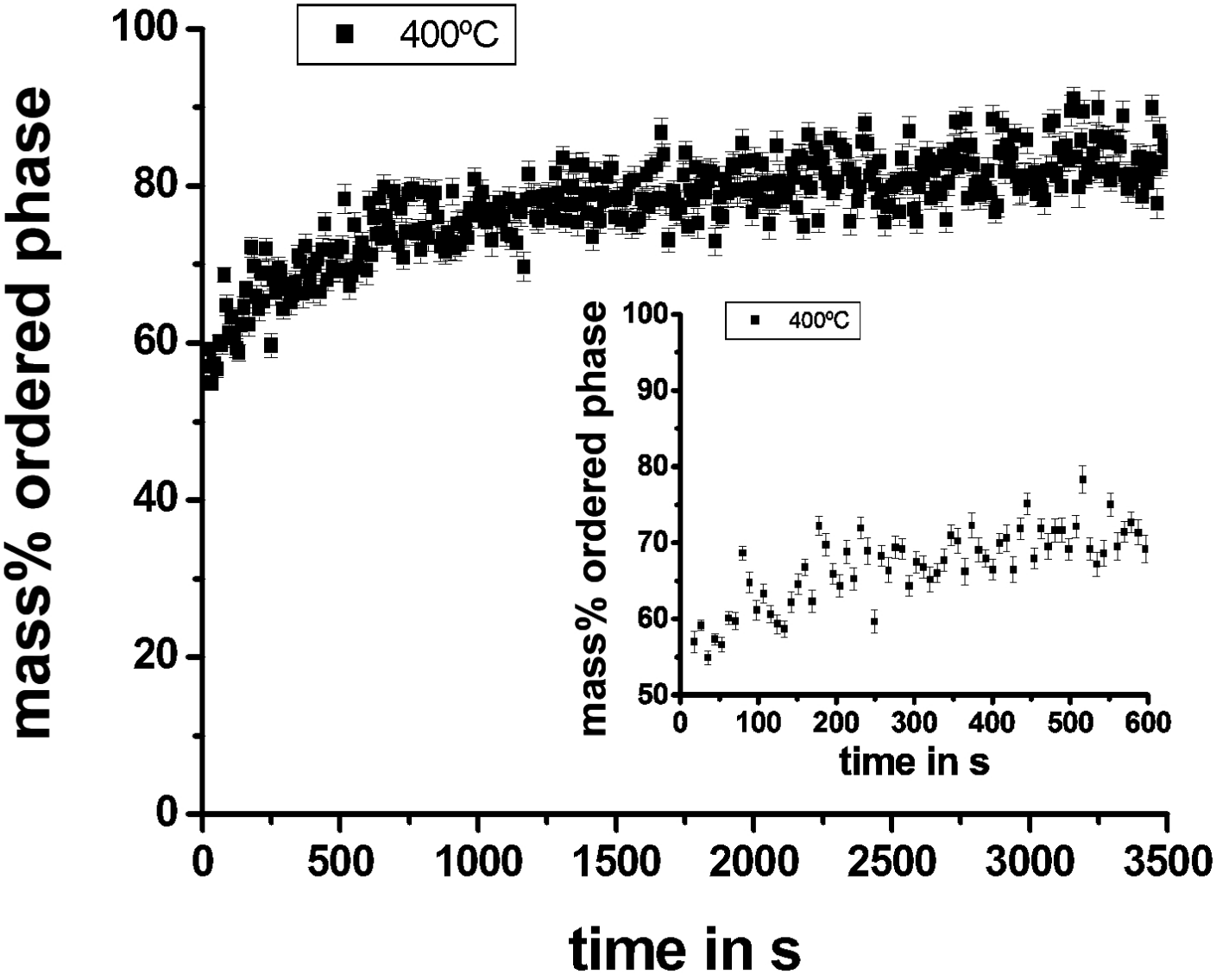
400°C
mass% ordered phase
time in s
0
20
40
60
80
100
0
500
1000
1500
2000
2500
3000
3500
400°C
mass% ordered phase
time in s
50
60
70
80
90
100
0
100
200
300
400
500
600

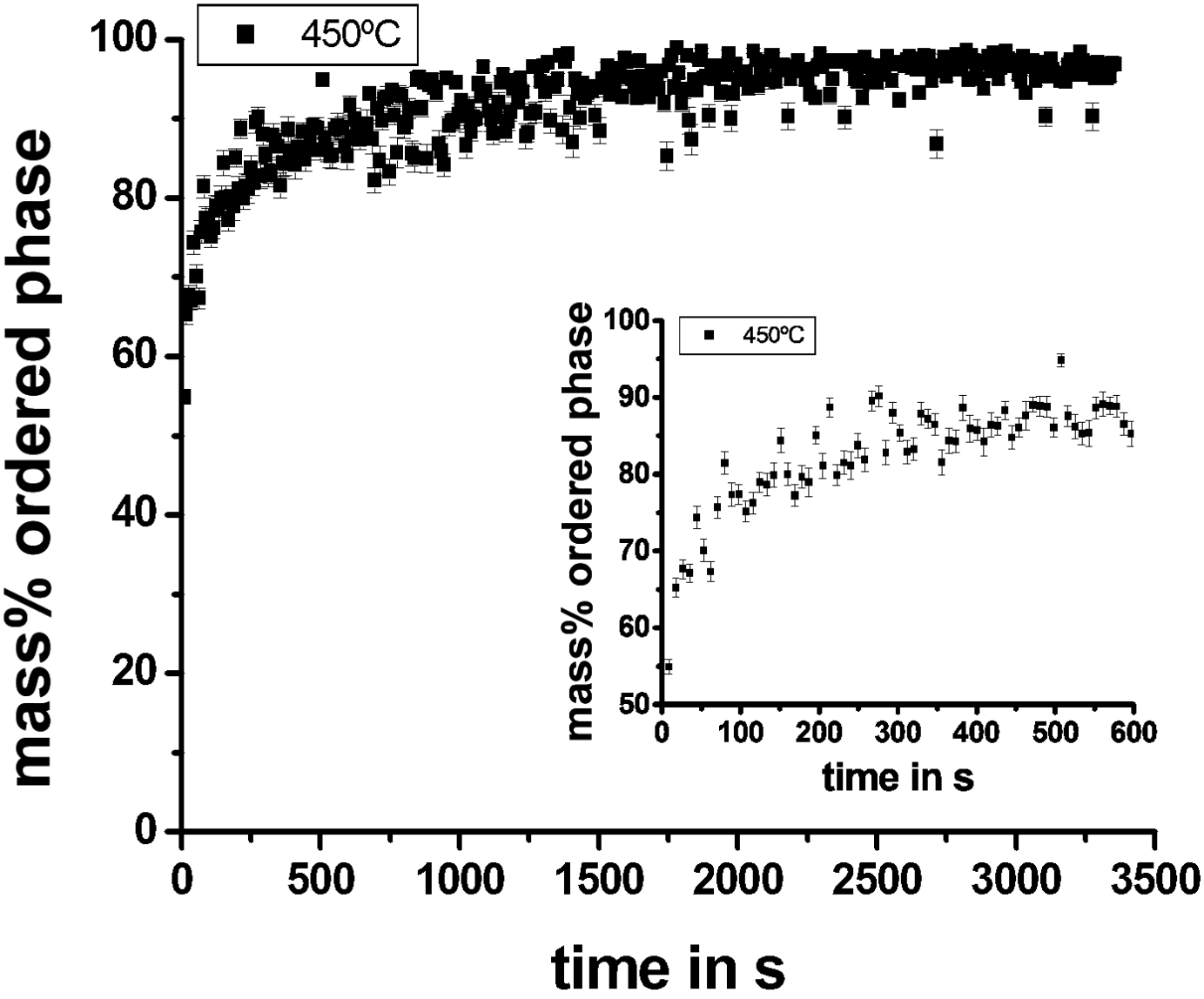
450°C
mass% ordered phase
time in s
0
20
40
60
80
100
0
500
1000
1500
2000
2500
3000
3500
450°C
mass% ordered phase
time in s
50
60
70
80
90
100
0
100
200
300
400
500
600

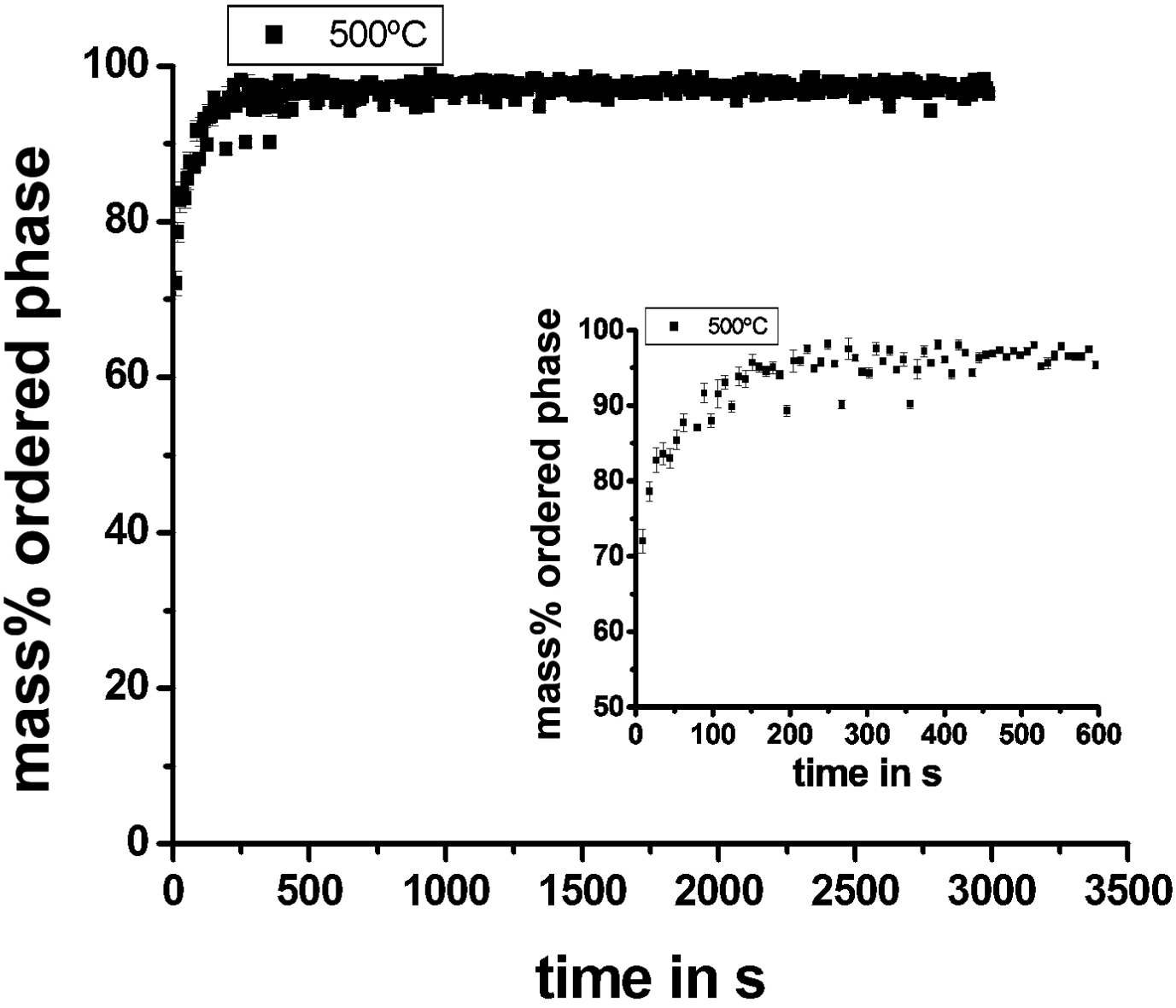
500°C
mass% ordered phase
time in s
0
20
40
60
80
100
0
500
1000
1500
2000
2500
3000
3500
500°C
mass% ordered phase
time in s
50
60
70
80
90
100
0
100
200
300
400
500
600

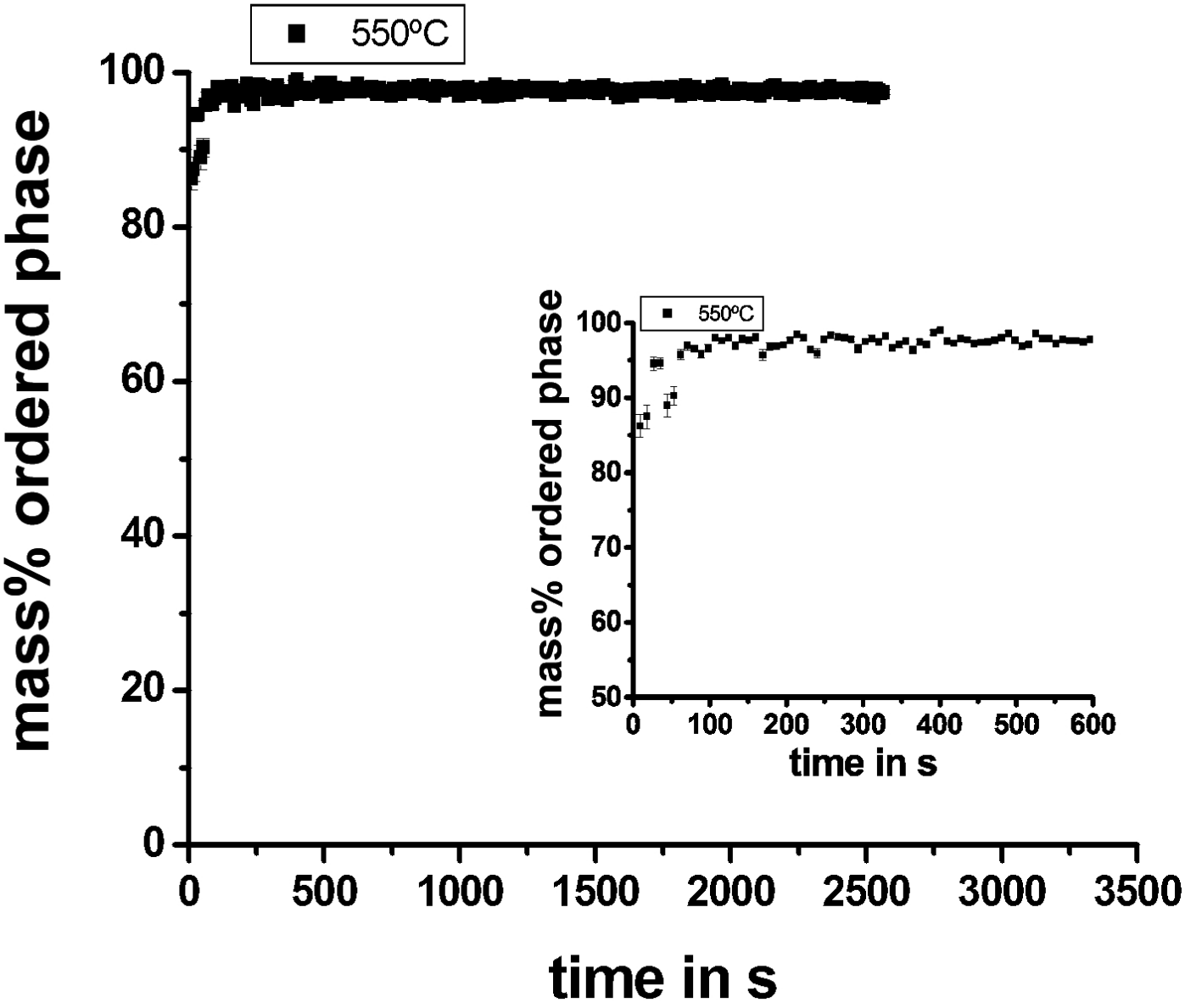
550°C
mass% ordered phase
time in s
0
20
40
60
80
100
0
500
1000
1500
2000
2500
3000
3500
550°C
mass% ordered phase
time in s
50
60
70
80
90
100
0
100
200
300
400
500
600

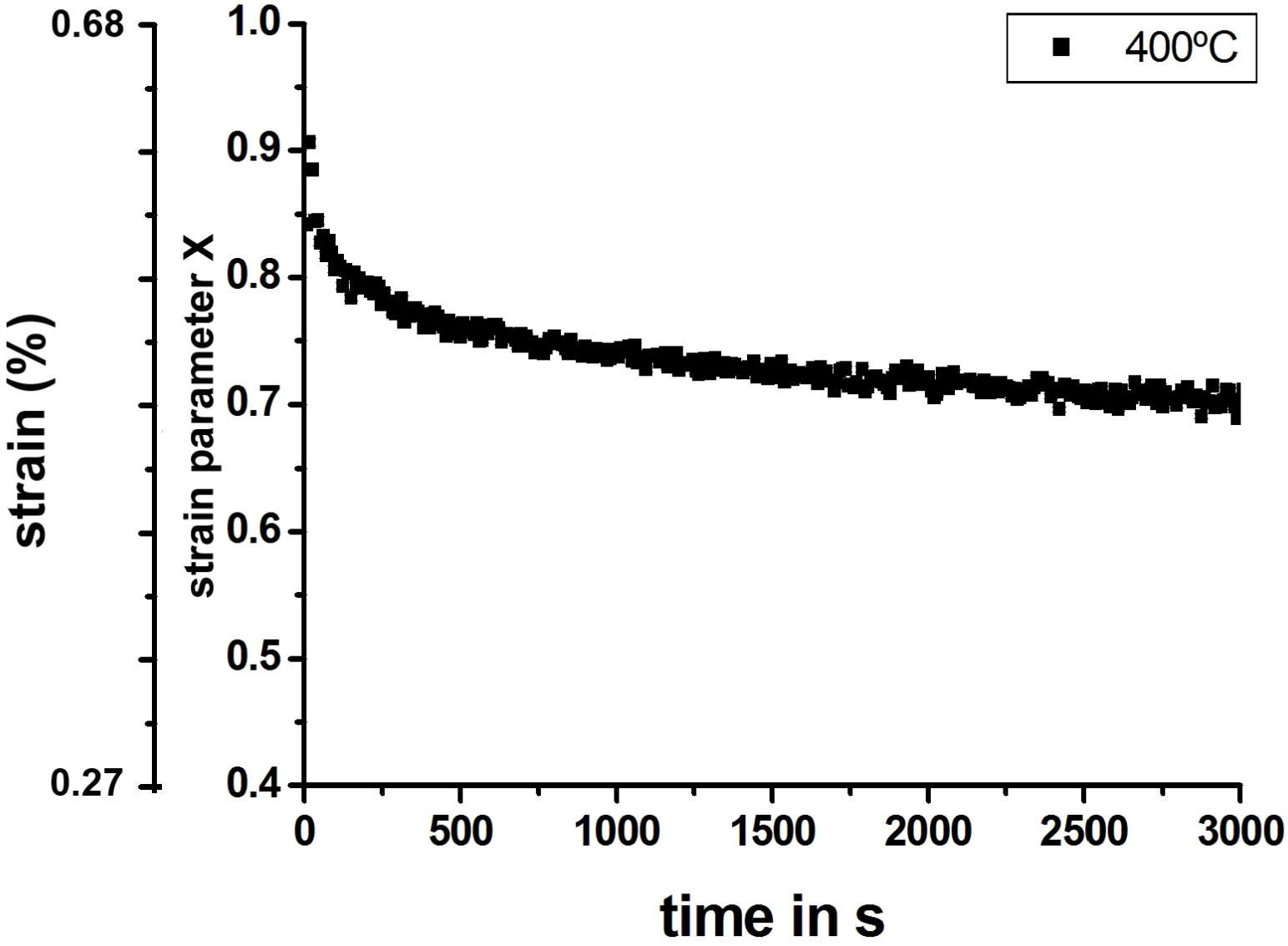
0.68
0.27
strain (%)
1.0
0.9
0.8
0.7
0.6
0.5
0.4
strain parameter X
0
500
1000
1500
2000
2500
3000
time in s
400ºC

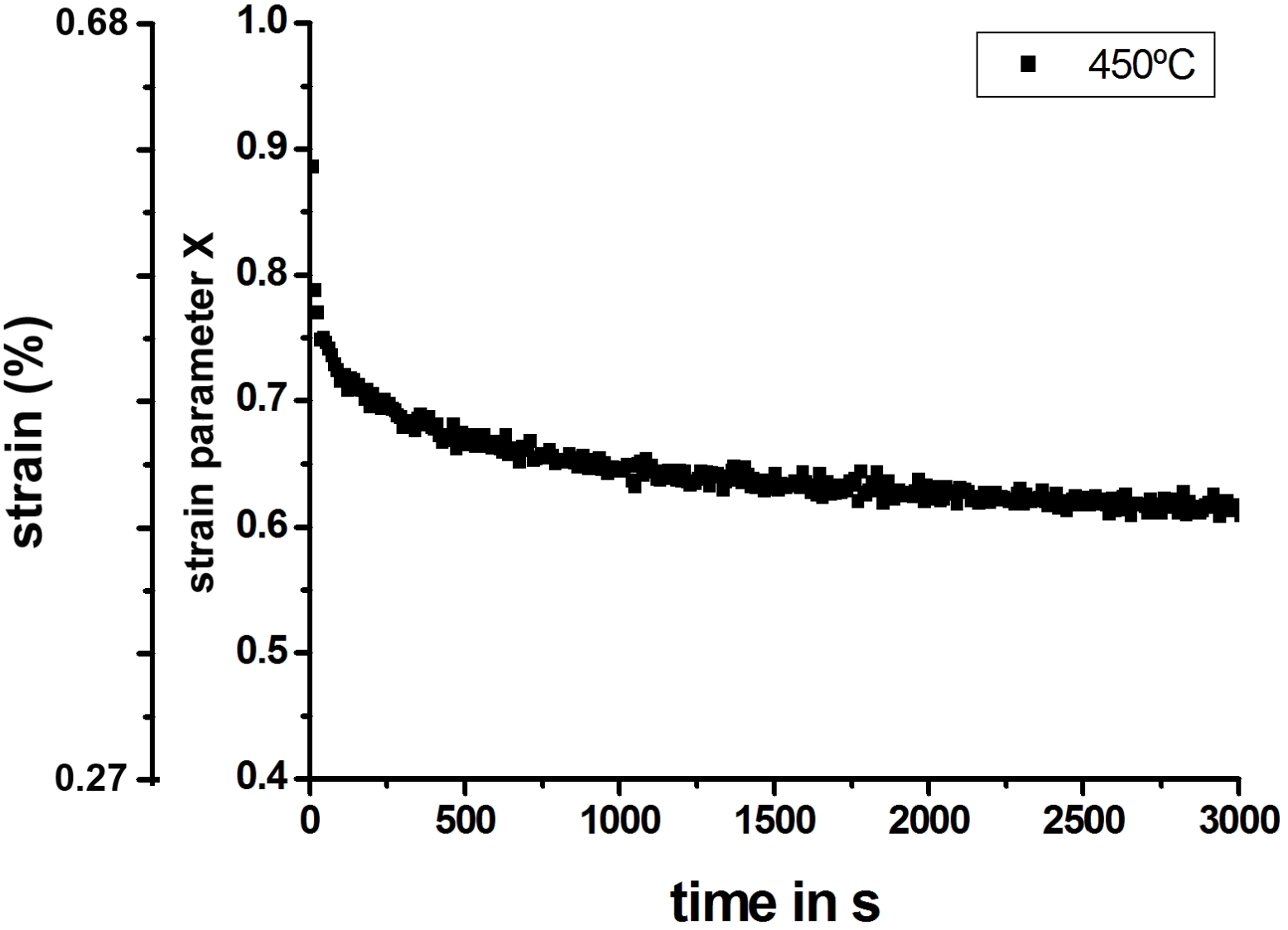
0.68
0.27
strain (%)
1.0
0.9
0.8
0.7
0.6
0.5
0.4
strain parameter X
0
500
1000
1500
2000
2500
3000
time in s
450ºC

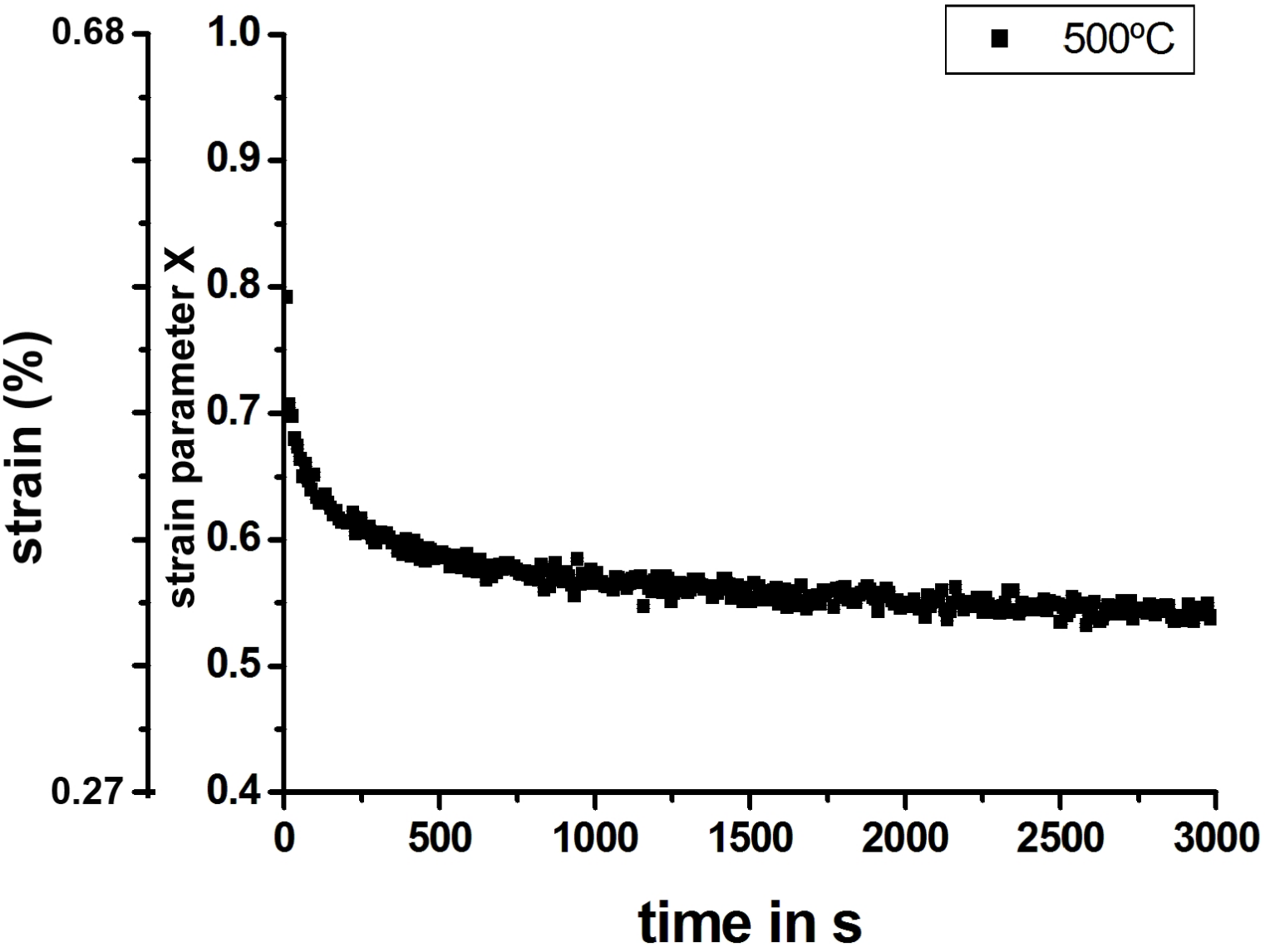
500°C
strain (%)
0.68
0.27
strain parameter X
1.0
0.9
0.8
0.7
0.6
0.5
0.4
0
500
1000
1500
2000
2500
3000
time in s

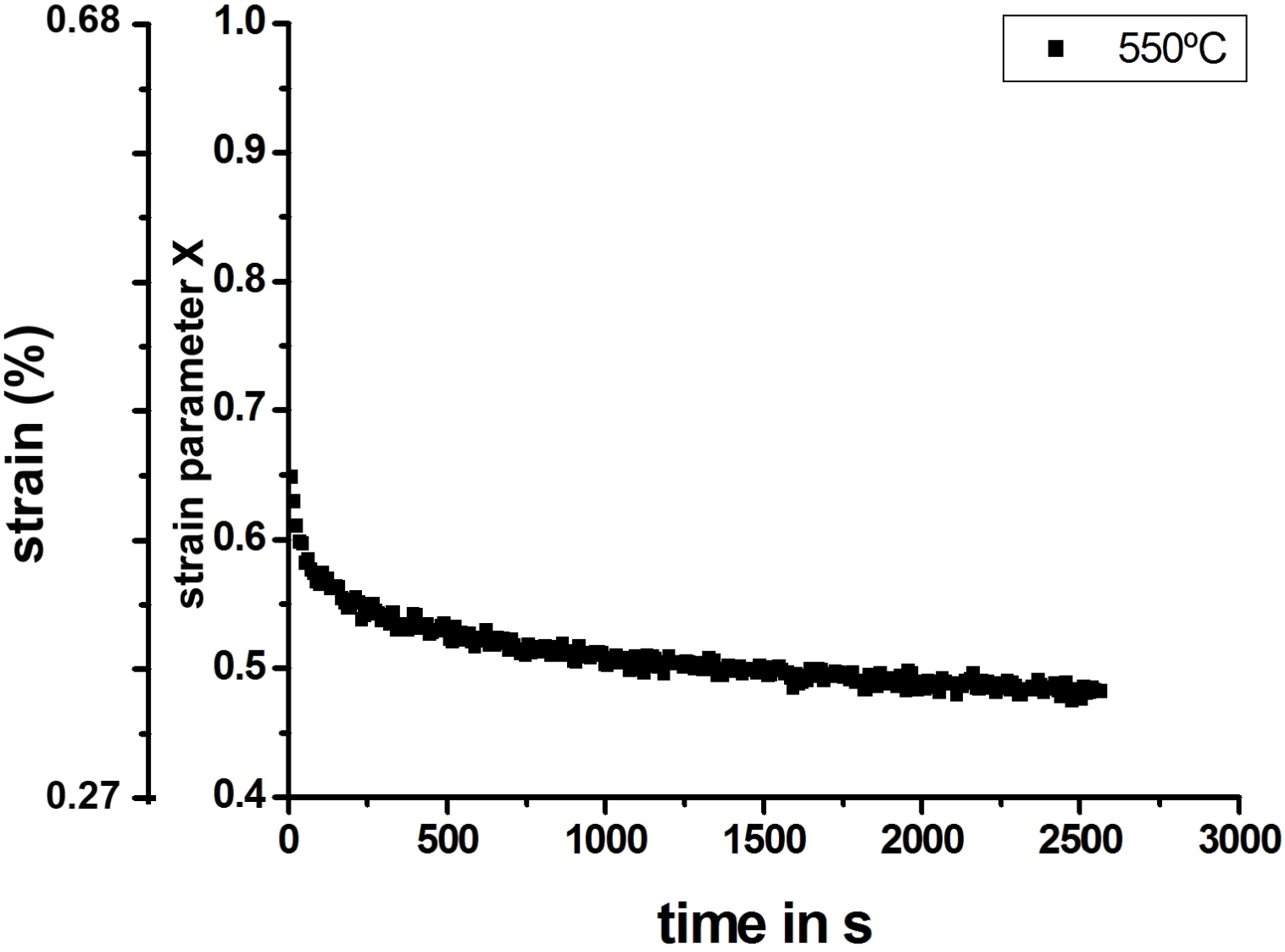
0.68
0.27
strain (%)
1.0
0.9
0.8
0.7
0.6
0.5
0.4
strain parameter X
0
500
1000
1500
2000
2500
3000
time in s
550ºC

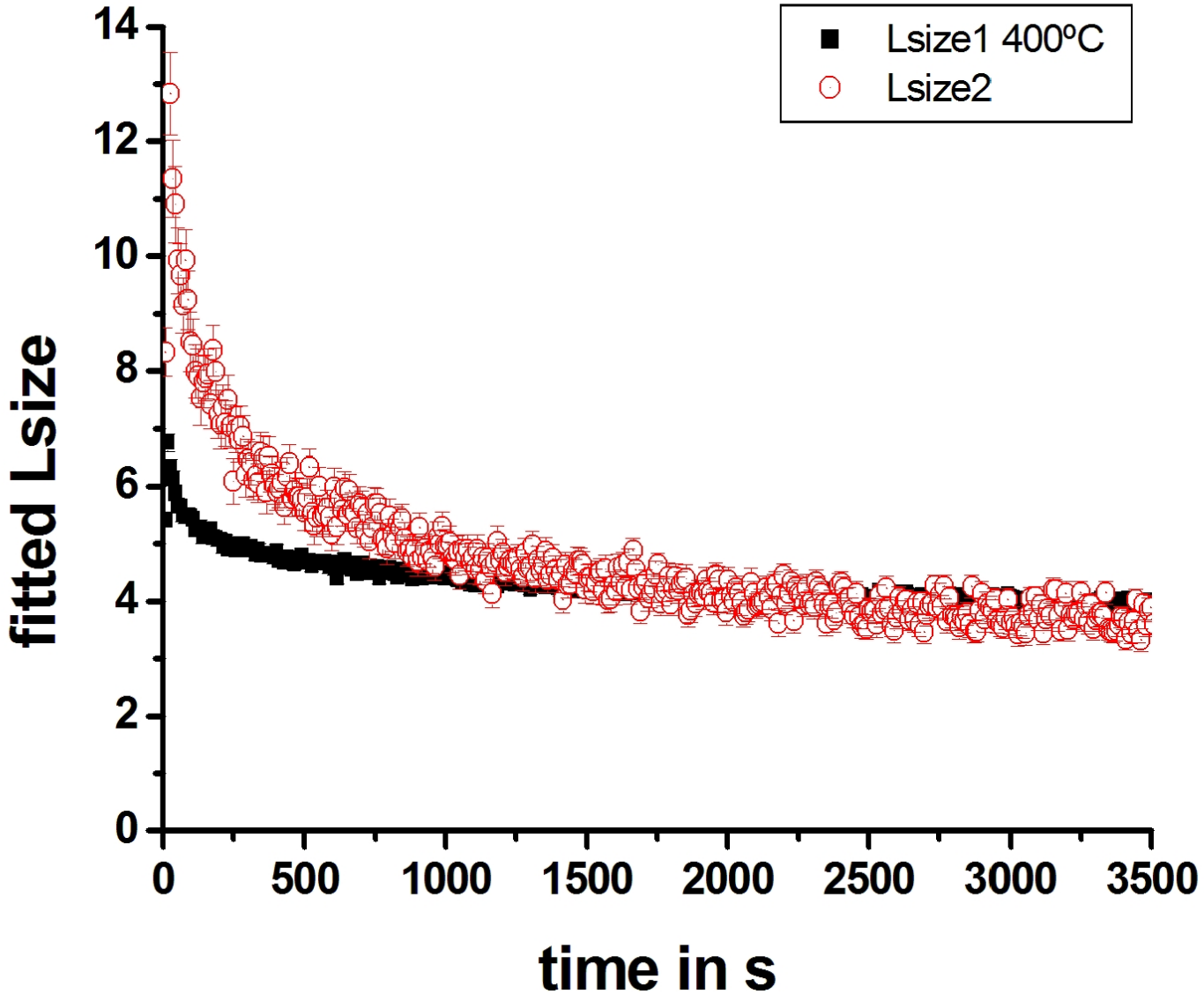
Lsize1 400ºC
Lsize2
fitted Lsize
time in s
0
2
4
6
8
10
12
14
0
500
1000
1500
2000
2500
3000
3500

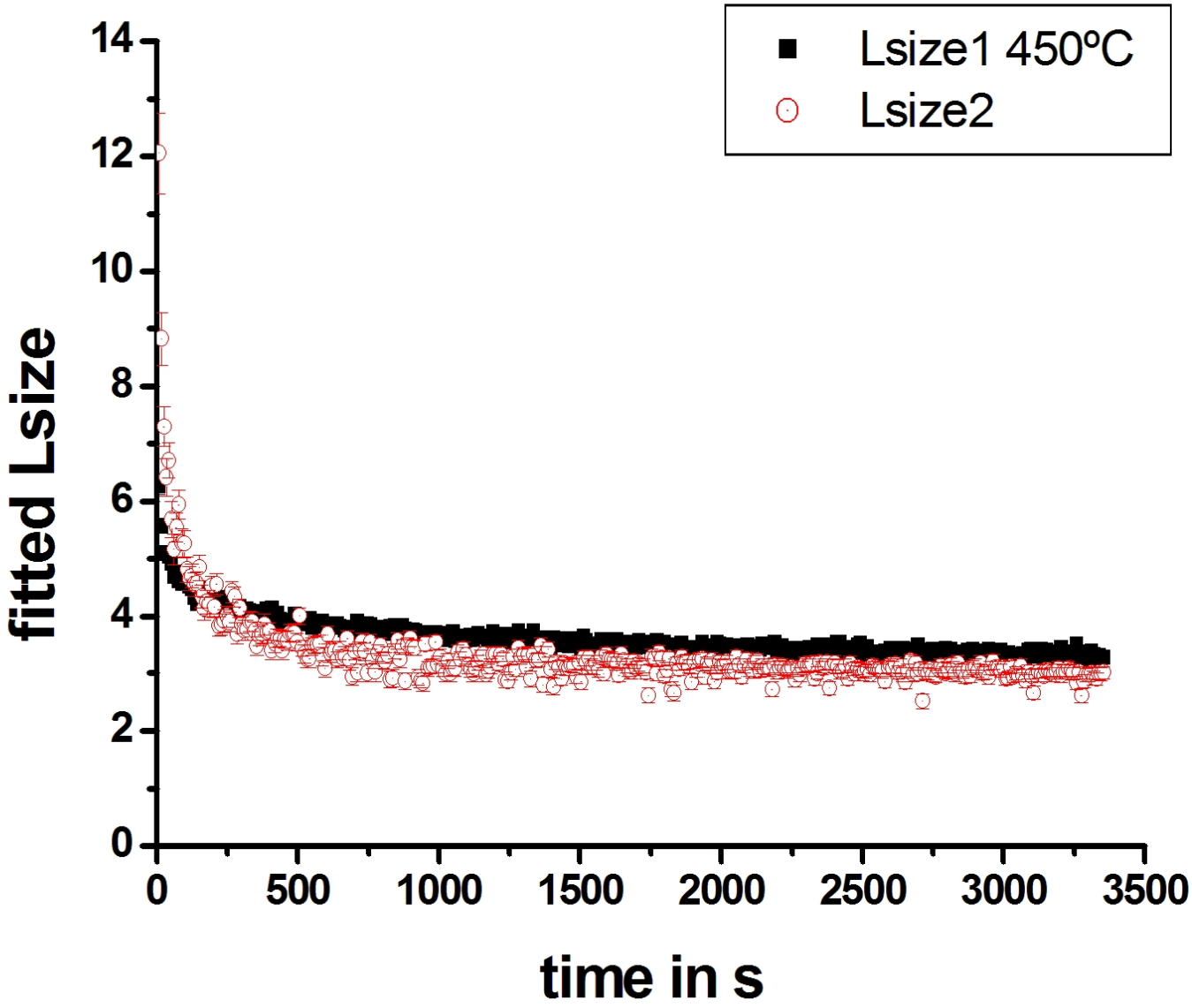
Lsize1 450ºC
Lsize2
fitted Lsize
time in s
0
2
4
6
8
10
12
14
0
500
1000
1500
2000
2500
3000
3500

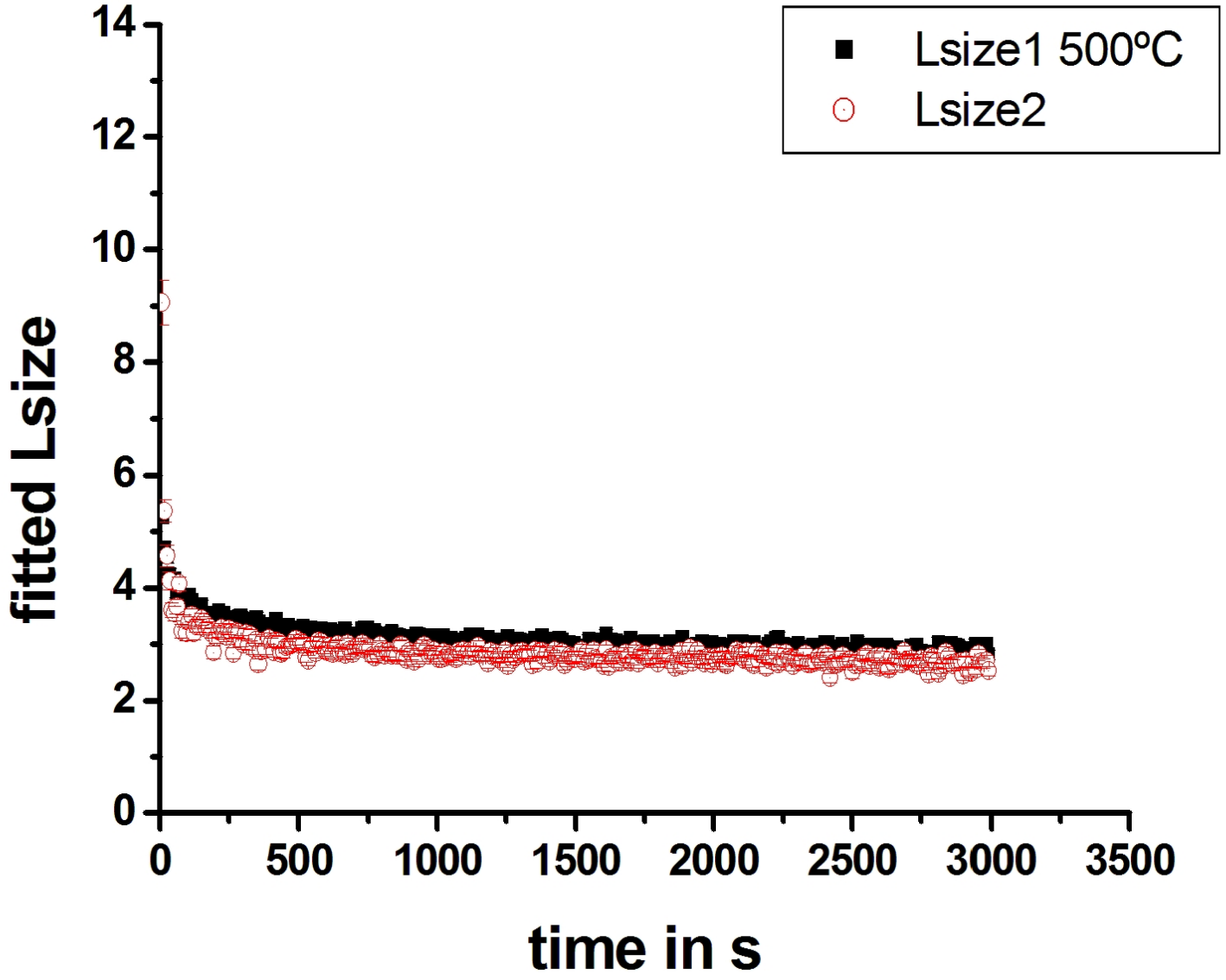
Lsize1 500ºC
Lsize2
fitted Lsize
time in s
0
2
4
6
8
10
12
14
0
500
1000
1500
2000
2500
3000
3500

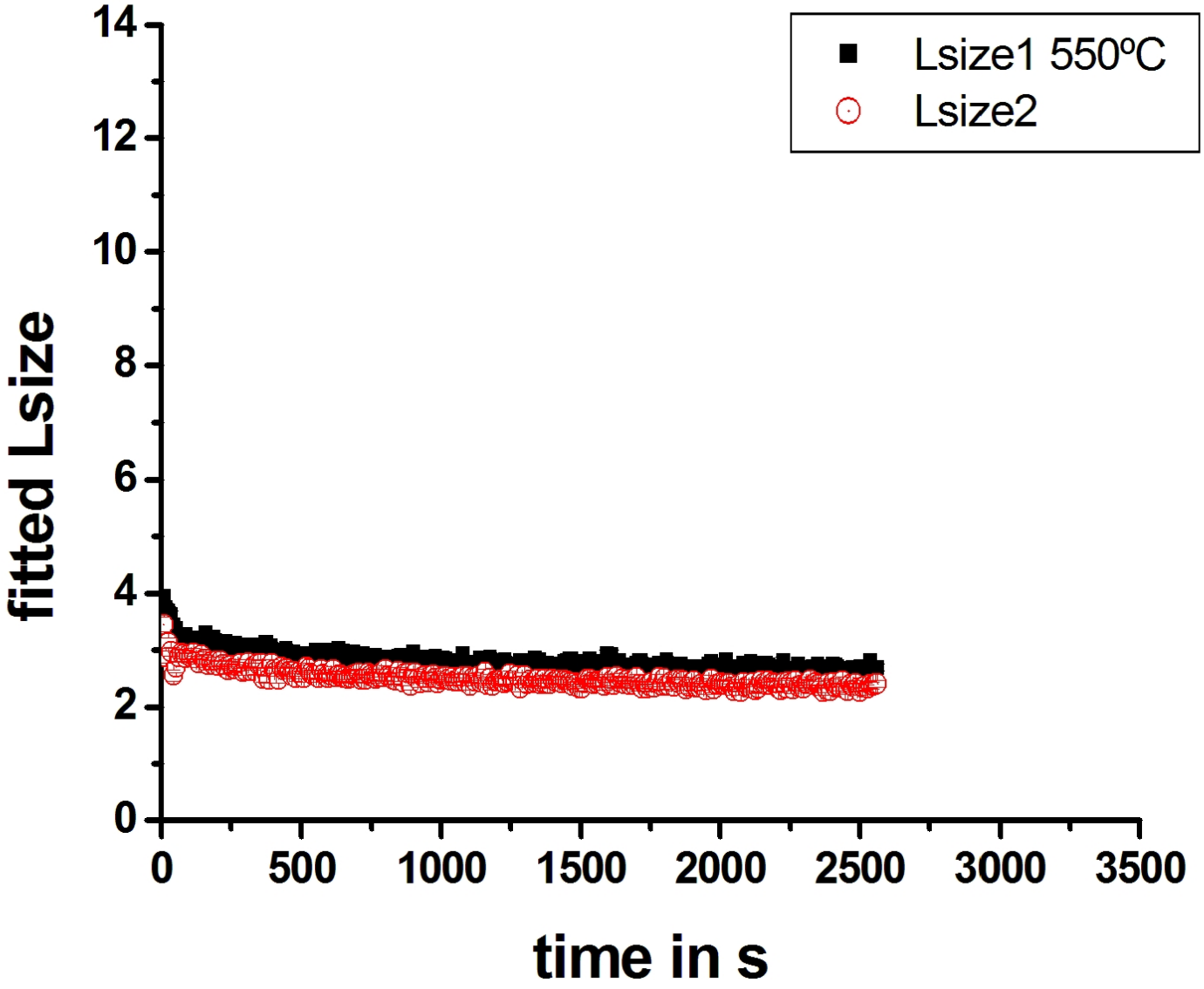
Lsize1 550ºC
Lsize2
fitted Lsize
time in s
0
2
4
6
8
10
12
14
0
500
1000
1500
2000
2500
3000
3500

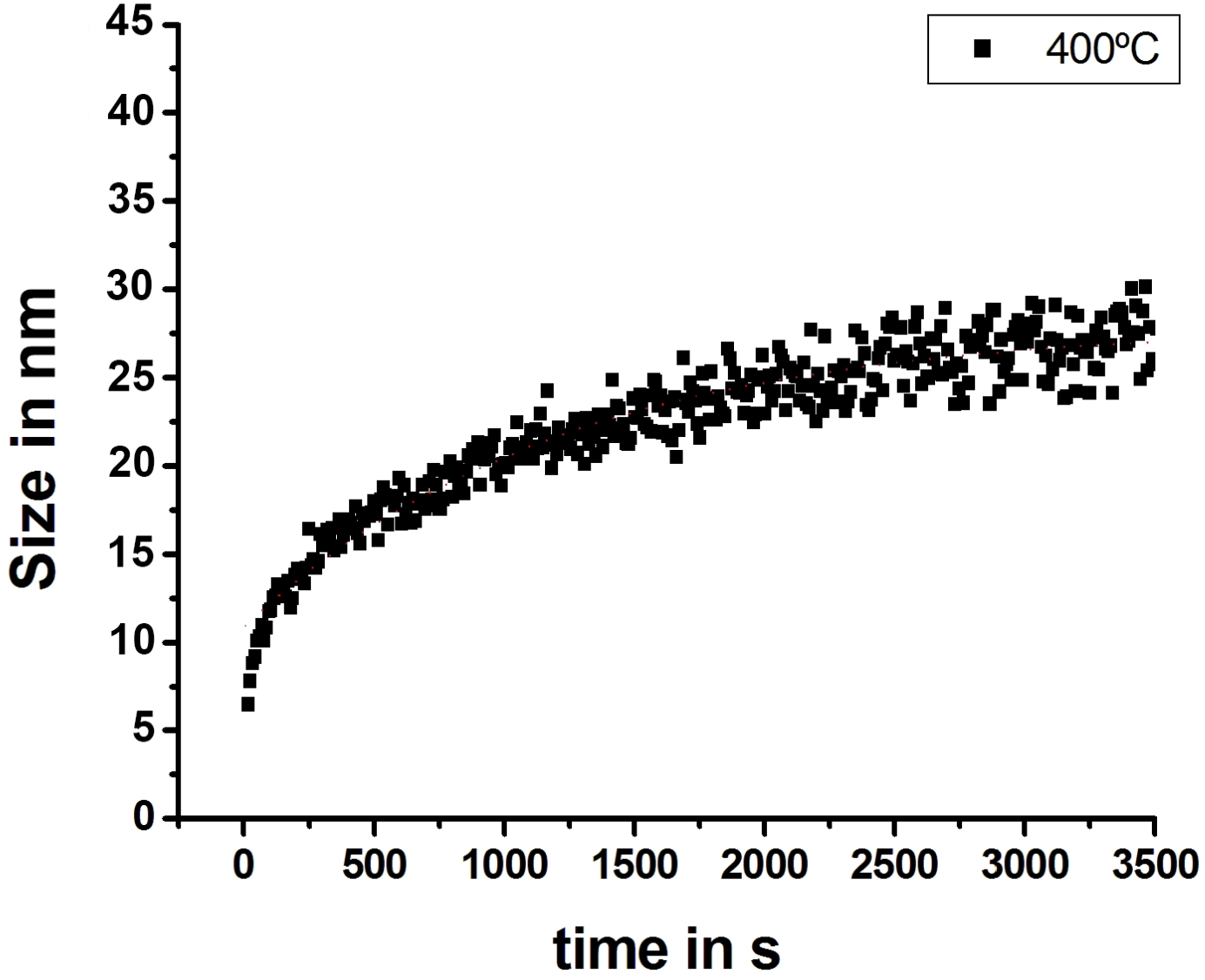
400ºC
Size in nm
time in s
0
5
10
15
20
25
30
35
40
45
0
500
1000
1500
2000
2500
3000
3500

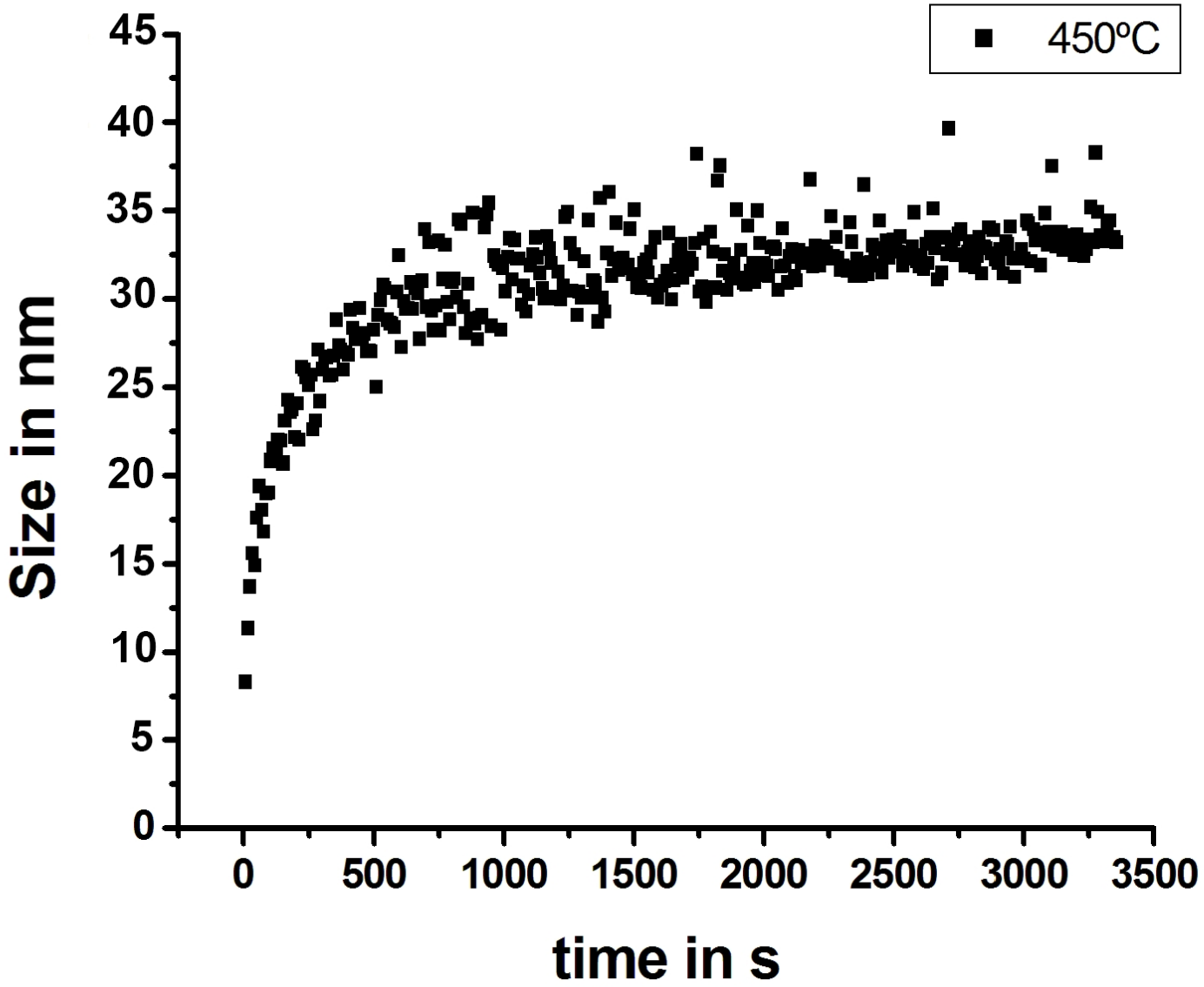
450ºC
Size in nm
time in s
0
5
10
15
20
25
30
35
40
45
0
500
1000
1500
2000
2500
3000
3500

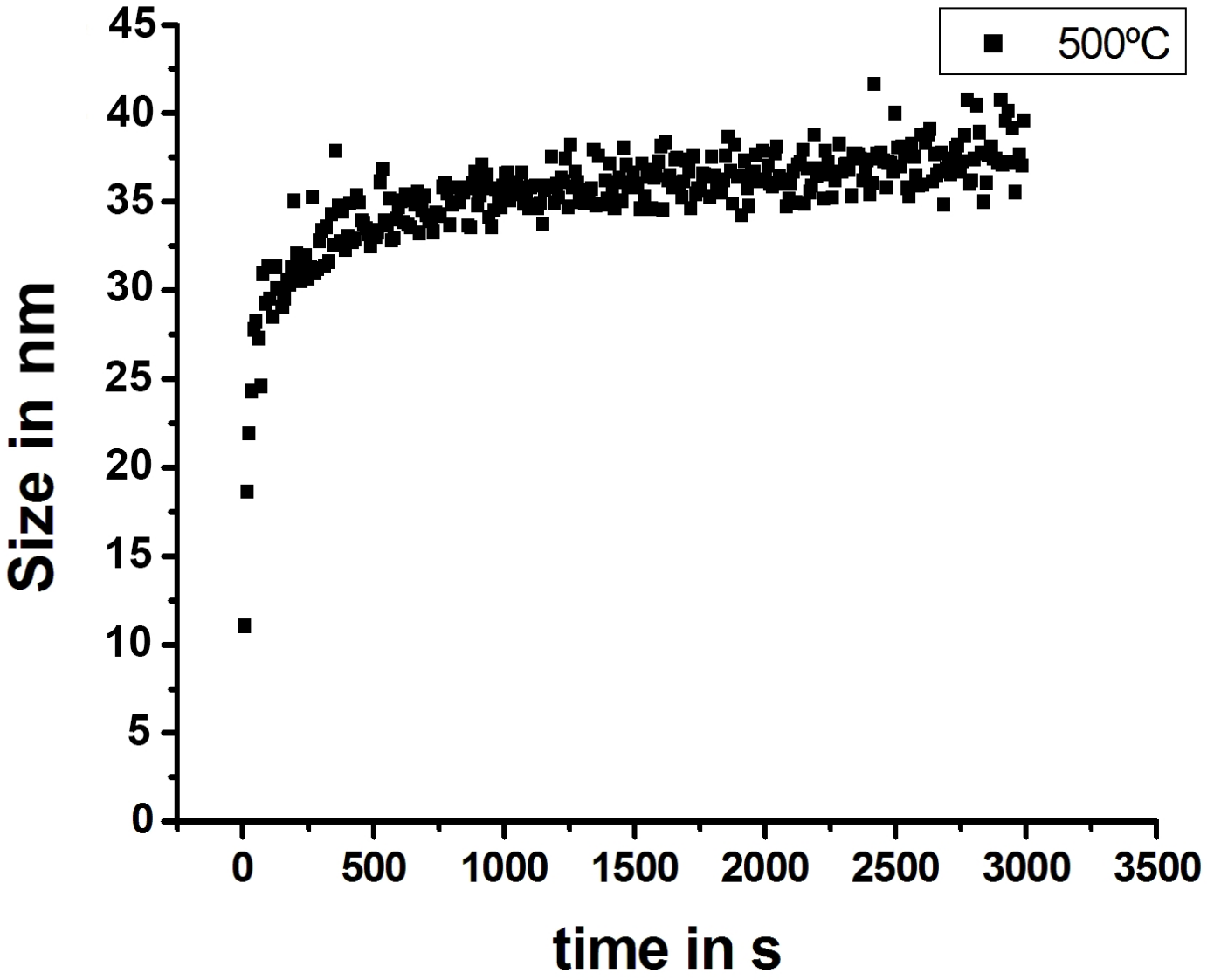
500ºC
Size in nm
time in s
0
5
10
15
20
25
30
35
40
45
0
500
1000
1500
2000
2500
3000
3500

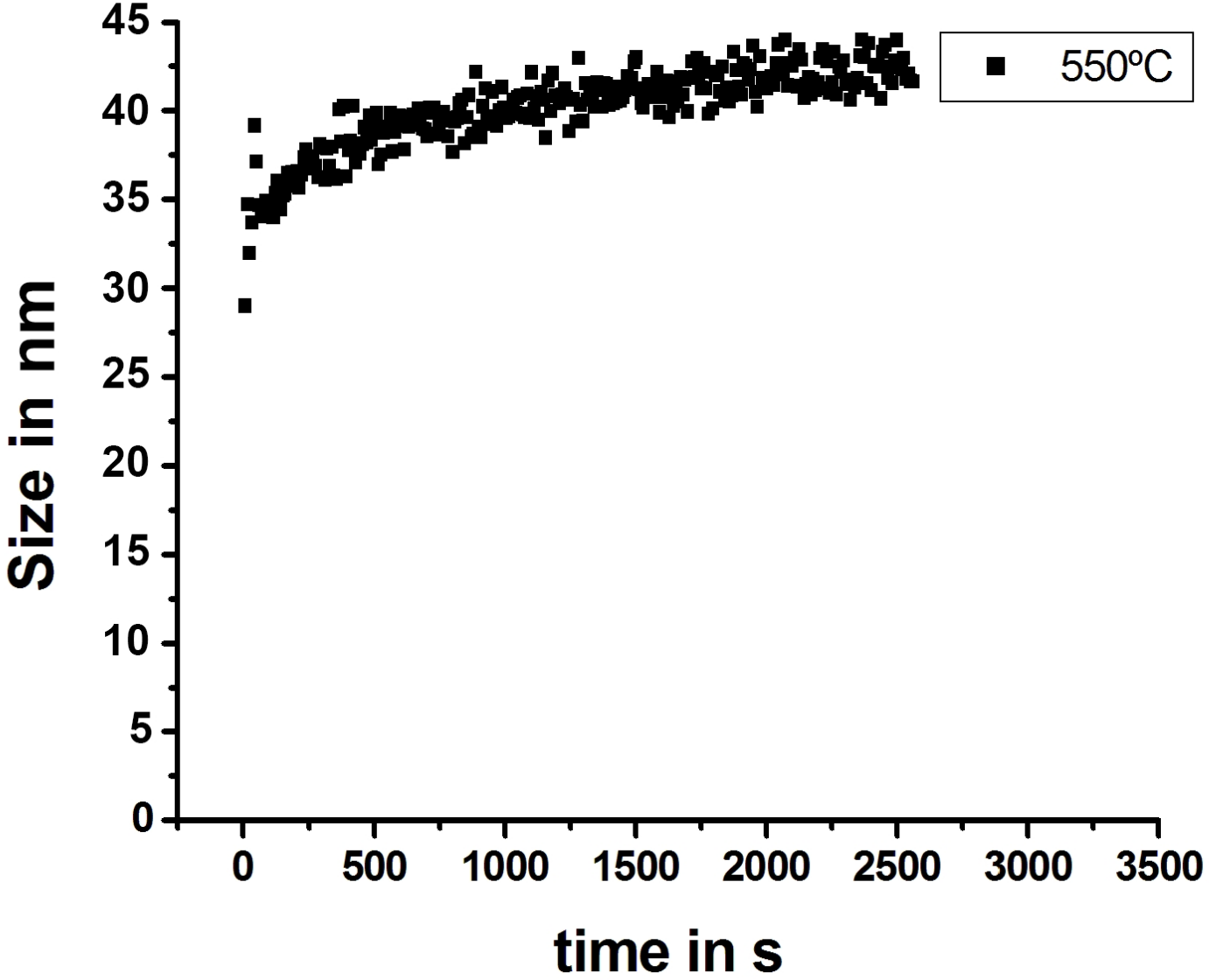
Size in nm
time in s
550ºC
0
5
10
15
20
25
30
35
40
45
0
500
1000
1500
2000
2500
3000
3500